공학석사 학위논문

Flexural Capacity and Behavior of Circular Concrete Filled Tube Beam-Columns without Axial Loads

원형 콘크리트충전강관 부재의 휨강도 및 거동

2017 년 2 월

서울대학교 대학원

건축학과

이 민 선

Flexural Capacity and Behavior of Circular Concrete Filled Tube Beam-Columns without Axial Loads

지도 교수 강 현 구

이 논문을 공학석사 학위논문으로 제출함
2016 년 12 월

서울대학교 대학원
건축학과
이 민 선

이민선의 공학석사 학위논문을 인준함
2017 년 2 월

위 원 장 이 철 호 (인)

부위원장 강 현 구 (인)

위 원 박 홍 근 (인)

Abstract

Flexural Capacity and Behavior of Circular Concrete Filled Tube Beam-Columns without Axial Loads

Lee, Minsun
Department of Architecture and Architectural Engineering
College of Engineering
Seoul National University

The use of concrete filled tubes (CFTs) with its own structural advantages has been used relatively recent comparing to other structural materials such as regular structural steel or regular reinforced concrete. Moreover, circular concrete filled tubes (CCFTs) provide more effective confinement by circular steel tube, bond stress transfer, and shear reinforcement to the concrete fill than rectangular concrete filled tubes. However, most prior experimental researches have been done focusing on the concrete filled tube columns. Even though some of them have been considered under pure bending, those have been done only using small sized specimens. The aim of this study is to examine the flexural behavior of full scaled circular concrete filled tube (CCFT) beams. Moreover, it attempts to investigate the effect of end plate. Five full scaled specimens were used to examine the flexural behavior. One was thick walled steel tubes without concrete fill, two were thick walled CCFTs with and without end plate, and other two were thin walled CCFTs with and without end plate. The test results

about flexural behavior of CCFTs are shown with applied moment, displacement, steel and concrete strain at each location.

This study also collected all the test specimens from the prior researches and this current test to make a comparison between the measured flexural strength and calculated nominal flexural capacity of CCFT according to common methods such as methods according to the ACI, AISC and Eurocode 4. One of the reasons is that due to the complexity of calculation for circular shapes, it is difficult to hand calculate the flexural strength of CCFT following the methods except the plastic stress distribution method of AISC which provides the closed form equations. Another reason is that all these methods give different calculated nominal flexural capacities of CCFT. In this study, an effort is made to review and compare the codes to identify their differences and also develop a computing program for the nominal flexural capacity of circular concrete filled tubes under pure bending that is in accordance with the codes. The developed computing algorithm, which is programmed in MATLAB, is not only used to compare the measured and calculated flexural strength of CCFT in this study but also is used to generate design aid graphs for various steel grades and a variety of strengths of steel and concrete. The design aid graphs for CCFT beams can be used as a preliminary design tool.

Keywords : circular concrete filled steel tube, beam-column, nominal flexural capacity, flexural stiffness, design code
Student Number : 2015-21113

Contents

List of Tables

List of Figures

List of Symbols

A_{fr}	Frictional surface area along the span length, mm^2
A_c	area of concrete component, mm^2
A_s	area of steel component, mm^2
B	sectional width of rectangular-shaped CFT, mm
C_3	coefficient for calculation of effective rigidity of filled composite compression members
D	diameter of circular concrete filled tube, mm
E_a	modulus of elasticity of steel according to Eurocode 4, MPa
E_c	modulus of elasticity of concrete, MPa
E_{cm}	modulus of elasticity of concrete according to Eurocode 4, MPa
EI	effective stiffness of CCFT, $kN\text{-}m^2$
E_s	Young's modulus of steel, MPa
$F_{concrete}$	force of inner concrete, N
$F_{inner\ steel}$	force of imaginary inner steel, N
$F_{outer\ steel}$	force of imaginary outer steel, N

F_y	yield stress of steel, MPa
F_1	force of steel in the first zone of total circular concrete filled tube, N
F_2	force of steel in the second zone of total circular concrete filled tube, N
F_3	force of steel in the third zone of total circular concrete filled tube, N
F_4	force of steel in the fourth zone of total circular concrete filled tube, N
F'_1	force of steel in the first zone of imaginary inner steel, N
F'_2	force of steel in the second zone of imaginary inner steel, N
F'_3	force of steel in the third zone of imaginary inner steel, N
F'_4	force of steel in the fourth zone of imaginary inner steel, N
I_a	the second moments of area of the structural steel section according to Eurocode 4, mm^4
I_c	the second moments of area of the un-cracked concrete section according to Eurocode 4, mm^4
I_g	moment of inertia of gross concrete section about centroid axis, neglecting reinforcement according to the ACI code, mm^4
I_{sx}	moment of inertia of structural steel shape, pipe, or tubing about centroid axis of composite member cross section according to the ACI code, mm^4
K_c	correction factor for concrete according to AISC (see Eq. (4-5))
K_s	correction factor for steel tube according to AISC (see Eq. (4-6))
K_e	correction factor to be used in the design of composite columns

L	total span length of specimen, mm
L_i	chord length of the total circular concrete filled tube section, mm
L_o	chord length of the imaginary inner steel core, mm
M_B	moment capacity when there is no axial load as Figure 4-1-(a), N-mm
$M_{concrete}$	moment of inner concrete, N-mm
$M_{inner\ steel}$	moment of imaginary inner steel, N-mm
M_{peak}	maximum moment capacity of each specimen, N-mm
$M_{outer\ steel}$	moment of imaginary outer steel, N-mm
M_1	moment of steel in the first zone of total circular concrete filled tube, N-mm
M_2	moment of steel in the second zone of total circular concrete filled tube, N-mm
M_3	moment of steel in the third zone of total circular concrete filled tube, N-mm
M_4	moment of steel in the fourth zone of total circular concrete filled tube, N-mm
M'_1	moment of steel in the first zone of imaginary inner steel, N-mm
M'_2	moment of steel in the second zone of imaginary inner steel, N-mm
M'_3	moment of steel in the third zone of imaginary inner steel, N-mm
M'_4	moment of steel in the fourth zone of imaginary inner steel, N-mm
Z_{cB}	plastic section modulus of concrete at point B as shown in Figure 4-1-(a), mm^3

Z_{sB}	plastic section modulus of steel tube at point B as shown in Figure 4-1-(a), mm^3
a	distance of equivalent rectangular stress block, mm
a_{shear}	shear span depth, mm
c	distance from the extreme fiber to neutral axis, mm
d	outer steel diameter according to AISC, mm
d_1	distance from the extreme compression fiber to the point where the steel starts to yield in the compression region, mm
d_2	distance from the end of the first zone to the neutral axis, mm
d_3	distance from the neutral axis to the point where the steel starts to yield in the tension region, mm
d_4	distance from the end of the third zone to the extreme tension fiber, mm
f'_c	compressive strength of concrete, MPa
$f_2(y)$	stress of the second zone, MPa
$f_3(y)$	stress of the third zone, MPa
h	Diameter of the concrete section or inner diameter of the steel tube, mm
k	factor relating effective compressive strength of concrete
l_1	span length from the end of specimen to the nearest reaction point, mm
l_2	span length from the reaction point to the nearest loading point, mm
t	thickness of steel, mm

$t_{end\ plate}$	thickness of end plate, mm
r_i	radius of imaginary inner steel core of inner concrete, mm
r_o	radius of imaginary outer steel crust, mm
β_1	factor relating depth of equivalent rectangular compressive stress block to neutral axis depth according to the ACI code
β_{dns}	ratio used to account for reduction of stiffness of columns due to sustained axial loads according to the ACI code
θ	Angle that defines the location of the plastic neutral axis at the inner face of the steel, º
ε_s	steel strain when the steel starts to yield
ε_{cu}	maximum usable strain at extreme concrete compression fiber
λ	factor relating depth of equivalent rectangular compressive stress block to neutral axis depth according to the strain compatibility method of Eurocode 4
η	factor relating effective compressive strength of concrete according to the strain compatibility method of Eurocode 4

Chapter 1. Introduction

1.1 Introduction

A composite structural system is widely used for high-rise and long-span buildings or structures, as the composite system has several advantages over regular reinforced concrete and regular structural steel. This type of composite structure consists of steel reinforced concrete (SRC) and concrete filled tube (CFT). The CFT system has been used for columns, where the compression forces are dominant. Accordingly, previous researches have focused on understanding the column subjected to concentric or eccentric compression. However CFT beams subjected to the pure bending moment are also used for the bridges (Nakamura et al., 2009), as shown in **Figure 1-1**, due to their structural advantages and constructional benefits. In particular, CFT bridges offer advantages in vibration, interior maintenance of steel tubes, and the external feature of tubes, as well as the enhanced flexural strength of members.

Figure 1-1 The case of CCFT bridge (Nakamura et al., 2009)

As mentioned above, early development of CFT researches has focused on CFT beam-columns, so there is a lack of studies concerning CFT beams, although some studies of CFT beams have been conducted. Initially, the pioneering works of Furlong (1967) assume that the CFT under pure bending has no contribution from the concrete core, and recommend that the flexural capacity of the CFT beam be evaluated by the plastic moment of the steel tubes, unless local buckling has not occurred. However, recently it became clear that the filled concrete in CFT beams has compressive resistance that prevents the local buckling of steel tube, and furthermore by moving the neutral axis towards the compression side, influences the composite action of the beam. These facts have been collectively accepted, and associated investigations are still being conducted (Prion and Boehme, 1993; Lu and Kennedy, 1994; Elchalakani et al., 2001; Gho and Liu, 2003; Han, 2004; Han et al., 2006; Thody, 2006; Chitawadagi and Narasimham, 2009; Probst et al., 2010; Deng et al., 2010; and Lee et al., 2016).

However, almost all of these researches have been performed with miniaturized specimens, not with actual sized specimens (Lu and Kennedy, 1994; Prion and Boehme, 1994; Elchalakani et al., 2001; Mohri et al., 2001; Han, 2004; Han et al., 2006). Furthermore, even though the sectional shape of CFT is also an important factor that affects its behavior and the shape factor of the circular tube is better than the square tube, there are limited researches addressing the circular shaped CFT (CCFT). Only Wheeler and Bridge (2004) and Probst et al. (2010) have recently performed CCFT experiments with full-scaled specimens. In particular, recent research by Probst et al. (2010) concentrated on the circular shaped CFT, and concluded that the designed nominal flexural capacities based on the plastic stress distribution methods of AISC and Eurocode 4 are greater than the measured maximum flexural strength that was achieved by tests. They predicted that the probable main reason for this result is the size of specimens.

Therefore, the test program in this study was performed to supplement

additional tests of full-scaled CCFTs. The results from the current test program deal with the flexural behavior of full-scaled CCFTs with thick and thin walled steel tubes, compared with bare steel tube with thick wall. This study also attempts to determine the effect of end plate on the flexural behavior of the CCFT.

After the assessment of the current test, this study developed a computing program to estimate the nominal flexural capacity of the CCFT with high convenience and high accuracy. That is because it is more difficult to estimate the flexural strength of circular CFTs than rectangular CFTs, due to the complicated computation associated with a circular section. The preliminary computing program suggested reflected all the differences between codes that were not consistent in design philosophy, or in recommendations of material or section, despite being available for composite structures worldwide, so the suggested program provides a meaningful tool to compute the flexural capacity of the CCFT according to many available methods. In this study, the strain compatibility methods (SCMs) of ACI, AISC, Eurocode 4, and the plastic stress distribution methods (PSDMs) of AISC and Eurocode 4 are addressed, and the differences of these methods are explained in **Chapter 4**. **Chapter 4** explains the algorithm that was applied to the program, and also shows the design aid graphs through the program.

To verify the proposed program and to compare the computed flexural capacity of CCFT with the measured values from tests, the specimens from previous researches are reviewed. From the outcomes of this comparison, this study evaluates each method. Furthermore, even though the flexural capacity of CCFT merely represents one point of the axial load-bending interaction curve (P-M curve) for beam-columns, it is meaningful to exercise in itself in order to obtain the value with a high degree of accuracy. It is significant not only to determine the nominal flexural capacity of CCFT beams, but also to describe each point in a P-M curve.

1.2 Objectives and scope

The major objective of this thesis is to determine the flexural behavior of CCFTs. Many researches focusing on this have already been performed, but until now, researches on the flexural behavior of CFT without any axial load have been restricted; and also, the researches for the flexural behavior of CCFTs have been even more limited. Furthermore, most of the prior researches have dealt with small-scale CCFT specimens. Therefore, this study concentrates on the tests of CCFTs subjected to no axial force with full-scaled specimens, and determines the flexural behavior of actual size CCFTs under pure bending. The current test also aimed to investigate the end plate effect on the flexural behavior of CCFTs. A total of 5 specimens were tested, which included 2 thick-walled CCFTs that had about 20 D/t ratio with and without end plate; and 2 thin-walled CCFTs that had about 42 D/t ratio with and without end plate, where D means the diameter of CCFT or steel tube and t means the thickness of steel tube.

Then, this study attempts to produce the design aid graphs for the nominal flexural capacity of the CCFT. This study examines the inconsistent design codes for CCFT beams, so firstly it determines the differences between many codes that are commonly used worldwide, such as ACI, AISC, and Eurocode 4. Through reflecting all these differences, **Chapter 4** proposes and explains a preliminary suggested program with a new algorithm. The outcome, i.e. the design aid graphs, is presented in the same chapter.

The final aim of this study is to compare the measured and calculated flexural capacity of CCFTs, so the proposed program is used to calculate the nominal flexural capacity of CCFTs according to each code and each method. Finally, the results of the calculated nominal flexural capacity of CCFTs through the program are compared with the results of the measured peak flexural capacity of CCFTs from real experiments. From the results of this comparison, this study evaluates each design method.

The specimens used for comparison between the measured and calculated flexural capacity of CCFTs are compiled from all prior researches that have been published, together with the current test. However, if the specimens were fabricated using special techniques, such as spiral welding, or with special material properties, such as self-consolidating concrete (SCC), or for other special reason seemed to be beyond the scope of this enquiry, the corresponding specimens were excluded. A total of 13 specimens were gathered, and these specimens were between 152 and 457.2 mm in diameter, and between 1.65 and 22.86 mm in thickness. The specimens also have a D/t ratio of between 19.97 and 92.12.

1.3 Organization

This thesis is organized into five main chapters. **Chapter 1** explains the importance and emphasis of the thesis and it shows the overall organization. **Chapter 2** explains in more detail prior researches on the behavior of CFT beam-columns, and in particular, previous researches on the flexural behavior of CFT beams. **Chapter 3** includes the assessment of the experimental program and results. The current experiment was conducted by the research team of Prof. Kang and Prof. Ramseyer in the Donald G. Fears Structural Engineering Laboratory at the University of Oklahoma. **Chapter 4** explains the differences of each method, and shows the suggested computing program that reflects all the differences of each method to estimate the nominal flexural capacity of the CCFT. Moreover, it compares with the measured value of the flexural capacity for CCFT specimens. **Chapter 5** then concludes the paper.

Chapter 2. Literature Review

In this chapter, the research history of CFTs is traced, together with the structural advantages of the CFT. The significant features of flexural behavior for CCFTs are also presented that are the main topics of the study.

2.1 General overview

The CFT is a composite structure that offers the benefits of both concrete and structural steel. The structural advantages of CFTs have meant that they have gained popularity, so CFTs have been used relatively recently compared to other structural materials, such as steel or reinforced concrete. The general mechanics, which means the main structural advantages of CFTs, are that concrete fill delays the local buckling of steel tube (Matsui and Tsuda, 1987; Guo et al., 2007), while the steel tube confines the concrete (Schneider, 1998). Moreover, CFTs also have many other structural benefits, such as increase of fire resistance performance, and decrease of concrete shrinkage or creep (Morino and Tsuda, 2003; Ying, 2006).

CFTs have not only structural advantages but also other advantages, such as cost performance and construction efficiency. According to Webb (1993), the building with CFT members has economical benefits, because the steel tube can be erected first and works as a frame member, which saves both construction time and cost. The concrete fill means that the quantity of steel material can be reduced with increase of building height. This aspect also leads to gains in economy and construction efficiency (Morino and Tsuda, 2003).

With the high popularity of CFTs, research on CFTs has also been activated. The United States and Japan first started a collaborative study to develop

seismic safety by using composite structures (Varma et al., 2002), and this joint research finally guided the first CFT design provisions of the Architectural Institute of Japan (AIJ) specification (Ying, 2006). After that, countless researches have reported on the performance of CFT members.

In particular, the main topics have been the bonds between concrete and steel, and the confinement of concrete infill. The radial displacement, shrinkage of concrete infill, and rugosity of the interior of steel tube affect the bond stress capacity, which is the transfer stress by bond between the two materials of concrete and steel. Schneider (1998) found that the confinement effects due to the steel tube are diverse according to the loading conditions. Fam et al. (2003, 2004) also demonstrated that the confinement by steel tube is a critical factor in the load resistance mechanism of the bonded CFT members.

The geometric characteristics that affect the behavior of CFT members, such as the thickness of steel tube, size of the CFT, and sectional shape, are also important factors. Many researchers reported that the D/t and L/D ratios are important factors for the performance of CFTs, where D means the diameter of CCFT or steel tube and t means the thickness of steel tube. Roeder et al. (1999, 2009) accounted for the circular-shaped concrete filled steel tubes (CCFTs) providing more effective confinement, bond stress transfer, and shear reinforcement to the concrete fill than rectangular-shaped steel tube. However, Wheeler and Bridge (2006) and Probst et al. (2010) pointed out that the researches with full-scaled specimens and under pure bending have been relatively limited, so there was a need to investigate real-size CFT beams with diverse sizes of CFT, and they conducted tests with actual size specimens. The details of these researches are explained in the following section with other notable researches about the flexural behavior of CFTs under pure bending.

There are many design codes worldwide for concrete filled tubes. The Korean Concrete Institute (KCI, 2012), American Concrete Institute (ACI, 2014), American Institute of Steel Construction (AISC, 2005), Eurocode 4 (EC 4,

1994), and Architectural Institute of Japan (AIJ, 2001) are the examples of design codes for CFT beam-columns. However, the design codes are not consistent in design philosophy, or in their recommendation of material or section, so the flexural capacity of CFT beams under pure bending also varies depending on each corresponding design code. The differences between each code and method are based on each assumption about the behavior of each material, and the interaction between each material. Chapter 4 discusses details of that difference between each code and method.

2.2 Previous studies

2.2.1 Researches on small scaled CFT

Tomii and Sakino (1979) tested 36 square-shaped (100 x 100 mm) beam-column CFTs, and only 4 among them were pure bending test specimen. The tubes were cold worked welded mild steel, and annealed at between 650 and 750 °C to remove residual stresses in the tube section. The yield strength of the tube was from 194 to 305 MPa, and the compression strength of concrete varied from 18.6 to 24 MPa.

Tomii and Sakino (1979) presented moment-curvature relationships for all the test specimens. However, this research was affected by initial CFT research, such as Furlong (1967), so they assumed that there was no slippage between the tubes and the concrete.

Prion and Boehme (1994) investigated the behavior of thin-walled CFTs. They used 26 specimens with 152 mm diameter and 1.65 mm wall thickness, which means that all the specimens were small-scale, so the diameter-to-thickness (D/t) ratio was 91. The specimens also had only 500 to 2,145 mm span, and the steel tubes were filled with high strength concrete that had 73 to 93 MPa compressive strength. The steel was cold formed, and its yield strength varied from 262 to

328 MPa. It was also welded with electric resistance longitudinal seams. Moreover, the specimens were tested under many load combinations ranging from pure axial compression, through combinations of axial load and bending, to pure bending. Only 5 specimens were tested under pure bending.

The applied loads to the beam specimens were concentrated at 2 central points, which induced a constant moment region between the loads. The distance between the point loads varied from 0 to 600 mm to investigate the shear effect on the bending capacities of the tubes, and according to the results, no definite trend in moment capacity was detected with the different spacing of loads. The applied load was cycled at about two to three times the yield deformation, until failure occurred. The moment-curvature relationships showed that the beam specimen under pure bending failed in a very ductile manner, by the rupture of the steel tube and buckling of the tube in the tension and compression region, respectively.

Therefore, the behavior of specimens under pure bending was normally ductile, but local buckling was detected around the reaction points. The push-out of concrete was also detected through the testing process, and at reach of failure. It was recorded about 1 mm before failure, and about 2 mm at failure. During the bending test, both ends of the CFT specimens were left uncapped, to allow slippage between the concrete and the steel. Prion and Boehme (1994) observed significant slippage between the concrete and the steel at each end, but reported that the slippage did not affect the strength of the CFT, but did affect the bending stiffness of the CFT specimens.

Prion and Boehme (1994) observed a remarkable increase in the carrying capacity in the beam specimen without axial loads, but a sudden decrease of carrying capacity when the applied axial loads were largely increased. They suggested that this aspect could be a promising topic for seismic resistance. The failure modes of beam-column specimens and that of beam specimen under pure bending were similar, so Prion and Boehme suggested that for the post

ultimate strength of CFTs, the CFT should be analyzed independently as concrete and steel.

Lu and Kennedy (1994) tested a total 27 beam-column specimens to determine the behavior of rectangular- and square-shaped CFTs. Among 27 specimens, pure bending tests were performed on 12 rectangular and square CFTs with 5 hollow tube (HT) beams for comparison with the CFTs. The main variables were depth/thickness (D/t), length/thickness (L/t) and shear span/depth (a_{shear}/D), so the values of depth, thickness and length were diverse. The depth value ranged from 152 to 252 mm, the thickness ranged from 4.8 to 9.4 mm, and the length from 2.0 to 4.3 m, respectively; but these dimensions mean that all the specimens were small scale. The steel tubes were cold-formed section with yield strength from 377 to 432 MPa, and the concrete strength ranged from 44 to 88 MPa. The applied load was monotonic with two-point loading, which provided a constant moment region.

The results of specimen from Lu and Kennedy (1994) concluded that the ductility in CFT beam specimens was drastically enhanced compared with hollow tube (HT) beam specimens. They reported that the moment capacity of CFT increased by about 23% on average with minimum and maximum increases of 10 to 30 % compared to that of HT alone. Not only the moment capacity, but also the stiffness of CFT was enhanced with 12% increase compared to HT specimen.

Moreover, HT beam failure was generalized by the downward buckling of the compression flange, and the outward buckling of the steel tube also occurring along the constant moment region. On the other hand, CFT failure was generalized by upward buckling and the occurrence of concrete crushing. The slippage was measured, but no notable slippage occurred during the test, and the shear span could also be negligible for the moment capacity. The neutral axis was observed during the test, and the test results presented that before the beginning of local buckling, the neutral axis rose; and after buckling occurred

in the steel compression flange, it was forced to shift downward.

Elchalakani et al. (2001) investigated the flexural behavior of CCFTs subjected to pure bending, with awareness of the lack of previous research. They focused on the *D* to *t* ratio ranging from 12 to 110. The diameter values were from 34 to 111 mm, and the thickness was from 1 to 3.3 mm, so all specimens were very small-scale. The specimens were loaded by two-point loading, and were uncapped to allow slippage between the concrete and steel tube.

Elchalakani et al. (2001) confirmed that the slippage between the concrete and steel was not detrimental, and the flexural capacity of CCFT was improved compared with the hollow steel tube. For example, the specimen with 31.15 *D*/*t* recorded a 37% increase in flexural moment capacity, while the specimen with 12.84 *D*/t recorded a 3% increase in flexural moment capacity.

Due to the above experimental results, Elchalakani et al. (2001) also suggested a design model for CCFT. Their model assumed that the bond between each material is perfect, and was based on the simplified rigid plastic approach as the plastic stress distribution method of AISC. Furthermore, they assumed that the confinement effect due to steel tube is perfect, so the compressive strength of concrete is also fully affected.

Mohri et al. (2002) researched the shear and flexural capacity of CCFTs. They used CCFT specimens that were of 200 mm diameter and 3.2, 4.5, and 6.0 mm thickness. SSK 400 was used for steel without reporting the yield strength, and 19.2 and 50 MPa compressive strengths of concrete were used as infill for low and high strength concrete, respectively. Ribs were installed to determine the bond capacity of the CCFT.

They attached strain gauges on the steel tubes, and reported the improved flexural behavior of CCFT compared to the bare steel. However, for CCFT specimens with ribs, the ribs accelerated cracks in the tension area of steel at the initial loading stage, so the results were that the ribs hindered the improved

flexural behavior of CCFT.

Han (2004) examined the flexural behavior of square- and rectangular-shaped CFT, focusing on three parameters, namely D/t, B/D, and a_{shear}/D. Sixteen specimens were used to determine the flexural behavior of CFT. The depths (D) of all specimens were 120 or 150 mm, breadths (B) (widths) of all specimens ranged from 60 to 120 mm, and the thicknesses (t) of all specimens ranged from 2.93 to 3.84 mm. The length of all specimens was 1,100 mm. Therefore the D/t ratio ranged from 20 to 50, the B/D ratio ranged from 1 to 2, and the a_{shear}/D ratio ranged from 1.67 to 2.1. However, all the specimens from Han (2004) were small-scale.

As a result of testing, Han (2004) presented that due to the concrete infill, rectangular- and square-shaped CFT beams showed great ductility, so the failure of all CFT specimens were ductile, and tensile fracture did not occur during the test. Han (2004) also concluded that the shear span was not a significant factor in the flexural behavior of CFTs.

Han (2004) compared the moment capacity of CFT with the predicted moment capacity according to AIJ (1997), BS5400 (1979), EC4 (1994), and LRFD-AISC (1999), and concluded that all the above stated codes estimate the moment capacity of CFT conservatively. For example, AIJ (1997) and LRFD-AISC (1999) provided flexural moment capacity that was about 20% lower than the measured value, BS5400 (1979) provided about 12% lower, and EC4 (1994) provided about 10% lower.

The research of Han et al. (2006) was a succession of the research of Han (2004), and this research focused not only on the D/t ratio and the shear span, but also on the different parameters, such as the cross-sectional shape and steel yielding strength. A total of 36 CFT beam specimens were used. The D/t ratio of all specimens ranged from 46.7 to 105.3, and the a_{shear}/D ratio ranged from 1.25 to 6. The thickness of specimens were 1.9 and 3 mm, and the diameter of

specimens ranged from 100 to 200 mm. Again in this research, all the specimens were small-scale. Three- and four-point loadings were applied, and self-consolidating concrete (SCC) was used for concrete infill, the compressive strength of which ranged from 51.5 to 81.3 MPa.

Han et al. (2006) presented in this research that the shear span-to-depth ratio neither affected the relationship of moment-curvature, nor the flexural capacity of square and circular shaped CFTs. Moreover, Han et al. (2006) compared the measured and predicted flexural capacity of CFT according to codes such as AIJ-1997, AISC-LRFD-1999, BS5400-1979, EC4-1994, and the suggested method in this study; and they concluded that EC4-1994 and the suggested method were the best methods to design the flexural capacity of CFT. Also Han et al. (2006) asserted that compared with regular concrete infill, the SCC infill did not affect the flexural behavior of CFT.

Chitawadagi and Narasimhan (2009) investigated the flexural behavior of CCFTs concentrating on the steel tube thickness, diameter of CCFTs, and compressive strength of infill concrete. They used 18 CCFT specimens of between 44.45 and 63.5 mm diameter, and between 1.27 and 1.98 mm thickness, so the D/t ratio was between 22.3 and 50.8. All the specimens were small-scale. The 20, 30, or 40 MPa compressive strength of concrete was used to infill the CCFT, and the yield strength of 250 MPa of steel tubes was used for CCFT specimens with spiral welding. All specimens with 1,000 mm length were tested under four-point loading.

Chitawadagi and Narasimhan (2009) noted that the flexural capacity of the CCFT developed according to the increase of diameter of the CCFT, and that of the thickness of steel tube. The increase of compressive strength of concrete did not significantly affect the flexural capacity of CCFT, but did affect the curvature. Furthermore, the higher effect on the increase of flexural capacity for CCFT was revealed for the thinner-walled CCFT, compared with the regular bare steel tube. Chitawadagi and Narasimhan (2009) also compared the

measured and predicted flexural capacities of CCFT according to AISC and Eurocode 4, and they concluded that both codes provide conservative design.

Deng et al. (2010) examined the flexural behavior of CCFT compared with the post-tensioned CCFT. A total of 4 specimens were used, and these consisted of one bare steel tube, two CCFTs, and one post-tensioned CCFT. The diameter of specimens ranged from 219 to 273 mm, and their thickness ranged from 3.7 to 9.3 mm, with D/t ratio ranging from 27.3 to 59.2. The specimens from Deng et al. (2010) were all small-scale. The compressive strengths of concrete, which was self-consolidating concrete (SCC), were 41 and 58 MPa, and the yield strengths of steel were 340 and 345 MPa.

Deng et al. (2010) demonstrated the improved flexural capacity of CCFT by 38.9% compared with the bare steel tube. The failure of CCFT, and CCFT with post-tensioning, showed large plastic deformation and rupture at the tensile flange. Moreover, concrete spalling also occurred at rupture. Comparing the CCFT, and CCFT with post-tensioning, post-tensioning improved the flexural capacity of CCFT by 6.5%. Furthermore, they observed that post-tensioning did not cause more slippage or moment near the interface.

2.2.2 Researches on full scaled CFT

Wheeler and Bridge (2006) examined the flexural behavior of thin-walled CCFT subjected to pure bending. A total of 6 specimens were used, and the specimens consisted of 2 HTs, and 4 CCFTs. The specimens also consisted of two types, one of 406 mm diameter and 6.4 mm thickness, and the other of 456 mm diameter and 6.4 mm thickness, which means that the specimens from Wheeler and Bridge (2006) were full-scaled. Thus the ratios of D/t and L/D ranged from 63.4 to 71.3, and from 8.33 to 9.36, respectively. The compressive strengths of concrete for infilling were between 40 and 56 MPa. The steel for tubes was produced using a cold rolled process with seamless wielding, and the

measured yield strength of steel was 551 MPa.

Wheeler and Bridge (2006) demonstrated that concrete infill increased the ductility and flexural moment capacity of the CCFT. Moreover, the concrete infill prevented detrimental deformation such as local buckling. The slippage between the tube and concrete was measured, and it was reported that slippage did not affect the flexural moment capacity of the CCFT beams, as the maximum slippage did not exceed 5 mm.

Thody (2006) and Roeder et al. (2009) studied the flexural behavior of thin-walled CFT. Thody (2006) used 9 specimens, while Roeder et al. (2009) used 4 specimens. All the specimens that were full-scale and were generally used in practical construction were of 405 mm diameter and 6.35 mm thickness, so the D/t ratio was 80. The self-consolidating concrete (SCC) used for infilling the tube ranged from 84.11 to 93.77 MPa. The steel had 525 MPa yield strength, and it was spirally welded.

Thody (2006) found there was a consistent failure process that consisted of audible cracking, buckling of the tube, tearing of the weld section, and decreasing of strength. He also demonstrated that compared with bare steel tubes, the flexural strength increased by 40% for CFTs. However, unlike his prediction, there were no substantial differences between capped, galvanized, and greased CFTs, compared with normal CFTs. Thody (2006) also tried to compare the measured flexural capacity and the predicted nominal flexural capacity depending on the methods of AISC. As a result, while the strain compatibility method (SCM) of AISC underestimated the flexural capacity of CFT by about 14%, the plastic stress distribution method (PSDM) of AISC did so by about 4%.

Roeder et al. (2009) also concluded that the CCFTs provided better flexural behavior than rectangular shaped CFTs (RCFTs). The reason was that the CCFT offers better confinement effects than the RCFT, so better bond stress between

steel and concrete was manifested, and offered better resistance against local buckling during the test.

Moreover, Roeder et al. (2009) argued that the efficiency of frictional bond stress is restricted to small D/t ratios and small diameter CFTs. The reason is that the frictional effects were not allowed, because of concrete shrinkage and the small radial stiffness of thin-walled CFTs. However, this excluded CCFTs with large bending moments, because binding action occurred, and no detrimental influence was developed for large diameter or D/t ratio CCFTs during large bending moments.

Probst et al. (2010) examined the flexural behavior of CFT without any axial force, and focused on the sectional shape of the CFT and the effect of shear connectors. A total of 4 specimens were fabricated, and the specimens consisted of 2 RCFTs with and without shear connector, and 2 CCFTs with and without shear connector. RCFT specimens were of 305 mm width, 405 mm depth, and 8.9 mm thickness, while CCFT specimens were of 457 mm diameter and 11.8 mm thickness. Furthermore, all specimens were of 6.1 m span, so these were full-scaled specimens that are used in practical construction. The measured compressive strength of concrete was 22.4 MPa, and the yield strengths of steel were 352 MPa for RCFT specimens, and 407 MPa for CCFT specimens.

Probst et al. (2010) supported the results of previous researches that the CFT beams behave with superior ductility and energy dissipation. Moreover, they reported that the shear connector in the RCFT did not substantially improve the composite action, while the shear connector in the CCFT increased the flexural capacity by about 40%. Likely because of the greater confinement and resistance to concrete radial shrinkage provided by the welded steel bars, the effect of the shear connector only influenced the CCFT specimen very well. However, at the ultimate state, the composite action for RCFT and CCFT specimens without shear connectors was not effective.

Probst et al. (2010) also compared the measured flexural capacity of CFT beams from experiment with that by calculation according to the AISC method and Eurocode 4 method. As a result, the measured flexural capacity of RCFTs exceeded that of the calculated nominal flexural capacity of RCFT, and also for CCFT beam with shear connector, the measured flexural capacity was greater than the calculated one; but for CCFT beam without shear connector, the calculated flexural capacity was greater than the measured one. In this aspect, Probst et al. (2010) asserted the need to consider the slippage between two materials of CFT more conservatively, so the methods from AISC and Eurocode 4, which assume that the perfect bond exhibits between concrete infill and steel tube, may not be proper to apply to CFT beams under pure bending.

Chapter 3. Assessment of Experimental Results

A full-scale experimental program was undertaken by the research team of Prof. Kang and Prof. Ramseyer in the Donald G. Fears Structural Engineering Laboratory at the University of Oklahoma. The current thesis provides a summary of the prior experimental study with more specific details that were not reported previously, and re-assesses the raw data to better understand the flexural behavior of CCFTs. A total of five CCFT specimens are used to investigate the flexural strength and corresponding ductility. The different flexural characteristics of thick- and thin-walled CCFTs are examined. Furthermore, the effect of the presence of end plates attached to both ends of each CCFT specimen is experimentally studied. The information regarding the test specimens, experimental set-up, and results is provided in the following sections:

3.1 Experimental program

This section describes all detailed information for designing the five specimens, and also describes the conditions of setup and other plans, such as gauges, linear variable differential transformers (LVDTs), and wire pots.

3.1.1 Specimen design

Table 3-1 briefly summarizes the five full-scaled specimens of 0.46 m outer diameter and 6.1 m long steel tubes that were fabricated. The individual characteristics of the five specimens are represented in the specimen labels. The first label denotes TK for the specimen with thick-walled tube, and TN for the specimen with thin-walled tube. The second label denotes CHT for the specimen of circular hollow tube, which means no concrete infill, and denotes

CCFT for the circular concrete filled tube. The third label denotes an additional EP when the end plates were attached.

Table 3-1 Dimension of specimens

	Designed Value			Measured Value		
Specimen	t [mm]	D [mm]	L [mm]	t [mm]	D [mm]	L [mm]
TK-CHT	19.05	457.20	6096	22.86	457.20	6121
TK-CCFT	19.05	457.20	6096	22.86	457.20	6401
TK-CCFT-EP	19.05	457.20	6096	22.86	456.18	6147
TN-CCFT	9.53	457.20	6096	10.16	455.93	6096
TN-CCFT-EP	9.53	457.20	6096	10.67	456.18	6121

First, TK-CHT, TK-CCFT and TK-CCFT-EP specimens were planned to have 6.1 m span, 0.46 m diameter, and 0.02 m thickness; while specimens TN-CCFT and TN -CCFT-EP were also planned to have 6.1 m span and 0.46 m diameter, but 0.01 m thickness. However, during the fabrication process, the dimensions of each specimen were changed, and **Table 3-1** shows the final actual dimensions, as mentioned earlier.

Two CCFT specimens of all five specimens were designed to attach end plates at both ends of the specimens by welding. **Figure 3-1** shows that to attach the end plate, two types of end plates with are for filling and ventilating, respectively, were welded for the concrete casting process. **Table 3-2** shows the thicknesses of the filling and ventilating end plates were the same.

Table 3-2 End plates

Specimen	Function of End Plate	$t_{end\ plate}$ [mm]
TK-CCFT-EP	Filling End Plate	20.07
	Ventilating End Plate	20.32
TN-CCFT-EP	Filling End Plate	12.95
	Ventilating End Plate	12.70

The size of 0.61 m by 0.61 m for steel plates and 101.6 mm standard threaded steel pipe angles were used to make the all end plates. A 0.1 m hole penetrated the lowest part of the filling end plate to allow the concrete infill to enter.

Another hole, which had also of 0.1 m diameter, penetrated the upper part of the ventilating plate and all these penetrations were made by plasma torch. After penetrating a pipe angle was joined to the holes of every end plate. All these weldings were fillet welds, and were also made by metal inert gas welder.

A perfect penetration should be assured for testing CCFT specimens with end plates on. Before fillet welding, both ends of the steel tubes were tilted at a 45° angle. It was necessary to secure the angle to get a suitable welding. For tilting the ends of a section, a plasma torch made rough faces, and a metal grinder was employed to smoothen the faces, and reduce the abnormalities before placing the end plates. The metal grinder was also used to remove the slags, which were from the fabrication process in the factory.

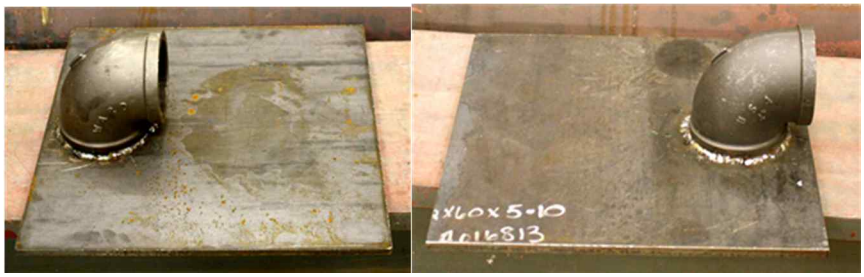

Figure 3-1 End Plates for Filling and Ventilating Concrete

3.1.2 Materials

CFTs consist of two materials, concrete and steel. Concrete for infill in the steel tube in this current test program was supplied with 34.5 MPa of compressive strength, 0.18 m of slump, and 0.01 m of maximum chip mix. However, no compressive cylinder achieved 34.5 MPa, as initially designed. **Table 3-3** shows that the maximum average compression strength of 29.5 MPa was achieved from the tested concrete cylinders. Furthermore, a 0.13 m slump was measured from the test, compared to the assumed 0.18 m slump.

Table 3-3 Results of compression tests of concrete

Cure time	Specimen	f'_c [MPa]	Average f'_c [MPa]	Failure description
7 Day	1	24.50	21.99	Chip failure at top
	2	50.55		Chip failure at bottom
	3	20.91		Chip failure at bottom
14 Day	1	21.94	17.51	Chip failure at bottom
	2	11.85		Chip failure at bottom
	3	18.78		Chip failure located on sides opposite each other
28 Day	1	25.80	24.34	Minor chip failure at 3371.60 psi on bottom, final failure resulting n cone failure top
	2	22.73		Chip failure at top
	3	24.41		Chip failure at top
124 Day	1	23.17	29.51	Chip failure at top
	2	31.12		Chip failure at bottom
	3	34.24		Chip failure at bottom

On the other hand, the yield stress of steel was measured as shown in **Figure 3-2**, and averaged by two coupon tests for each thick- and thin-walled steel tube. The yield strength of steel for thick-walled CCFT was 472.29 MPa and that of steel for thin walled CCFT was 455.05 MPa. The remarkable characteristics of steel material properties are that the plateau length of steel hardening from the steel coupon tests is long for thin-walled steel tube, and the slope of hardening is gradual for thick-walled steel tube.

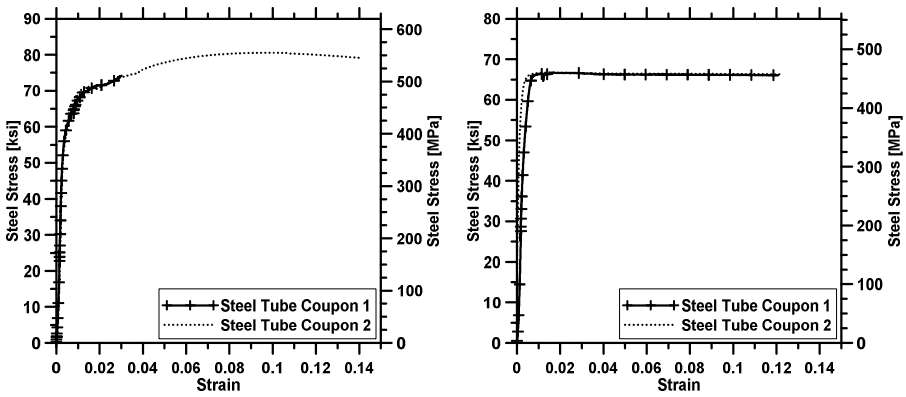

(a) For thick walled CCFT (b) For thin walled CCFT

Figure 3-2 Stress-strain curves of steel tube coupons

The CCFT specimens in this study are limited to the cases of CCFT compact sections according to the AISC code. The AISC code classifies the compact, noncompact and slender sections by the values of diameter to thickness ratios of the CCFTs. **Table 3-4** shows the boundary, and all the specimens in this study accorded with the compact section region.

Table 3-4 Limiting *D*/*t* ratio for CCFT beams (AISC 360-10)

Specimen	AISC 360-10		*D*/*t* (Measured Value)	
TK-CCFT	Compact/Noncompact	$\leq \frac{0.15E_s}{F_y}$	20.00	Compact Section $\leq \frac{0.15E_s}{F_y}$
TK-CCFT-EP	Noncompact/Slender	$\leq \frac{0.19E_s}{F_y}$	19.97	
TN-CCFT	Maximum Permitted	$\leq \frac{0.31E_s}{F_y}$	41.74	
TN-CCFT-EP			42.76	

3.1.3 Test setup

The test assembly consisted of the following: a reaction frame, a spreader beam, and a hydraulic ram. All testing was conducted on the reaction floor. In order to distribute the load, cradles were attached to all reaction points. The depth of

the cradles was measured to be 0.08 m and they were made specifically for 0.46 m circular sections, as shown in **Figure 3-3**.

Figure 3-3 Cradles before being attached

Specimens were loaded and unloaded using the shop 5,000 kg crane. The maximum calculated weight of the specimens was 3,175 kg. A safety brace was used that connected the spreader beam to the reaction frame, as shown in **Figure 3-4**. The brace restricted the horizontal moment of the spreader beam, and in the event of dramatic failure, would help carry the spreader beam safely. To measure the applied load, a 1780 kN load cell was used between the spreader beam and the hydraulic ram. Steel shims were placed between the ram and the load cell prior to and during loading.

Figure 3-4 Setting of the instrument for testing

Prior to loading the CCFT into the testing frame, nineteen strain gauges were applied at the mid-span of each beam to monitor the neutral axis, as shown in **Figure 3-5**. The gauges were placed every 0.03 m along the vertical axis. For all CCFT specimens, an additional strain gauge was attached above the reaction point at the plastic neutral axis (PNA) along the east and west side of each end as shown in **Figure 3-6**. A total of twenty-three strain gauges were required for each CCFT. Preparation of the steel surface for attaching each strain gauge involved carefully removing the mill scale, and any oils or impurities. For this, a disc sander was used, after which all polishing was done by hand. In order to clean the surface from containments, the surface was wiped with lacquer thinner, acid, and then base. Special non-stretch cellophane tape was used for the placement of each strain gauge. Once situated, the end of the tape was lifted up to expose the bottom of the strain gauge, after which a catalyst was applied directly to the strain gauge. Glue was then put on the steel surface, and the strain gauge was pressed down for 2 minutes to set. After setting, the cellophane tape

was removed, and the strain gauge was covered with a thin layer of silicone for surface protection. All strain gauges were prewired, and silicone caulk was used to mount all wiring to the steel tube for strain relief, in case of any accidental pulling on the wire.

Figure 3-5 Nineteen strain gauges attached around the specimen on the mid span

Figure 3-6 Nineteen strain gauges attached around the specimen on the mid span

For CCFTs with end plates, 2 LVDTs were placed at the top and bottom of both the north and south ends. LVDTs were placed flush with the exposed concrete to determine the amount of measurable travel of the LVDT as 0.01 m, as shown

in **Figure 3-7**. Wire pots were also used to measure the deflection at the mid-span of the empty section, and at the quarter-span and mid-span for all CCFTs, as shown in **Figure 3-8**. Two wire pots were located at each location along opposite sides, and were attached using magnetic hooks on the steel surface.

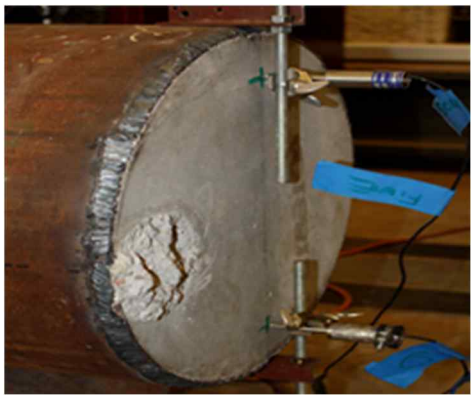

Figure 3-7 LVDT attached the end of specimen

Figure 3-8 Wire pots attached at the mid and quarter span of specimens

Figure 3-9 and **Table 3-5**, which illustrate the test setting, show that it was decided to test all CCFT beams with a constant region of 0.3 m and an increased shear span. This was done to increase the available applied moment. A new spreader beam was constructed, which was shorter, measuring 0.6 m in length.

TN-CCFT specimen and TN-CCFT-EP specimen were loaded twice, no complications arose during bending, and the beams were loaded smoothly. However, each testing for TK-CCFT and TK-CCFT-EP was performed over two days due to the high load needed from the hydraulic ram. This was done to let the hydraulic ram cool, as it was unable to sustain high loads for long periods at a time.

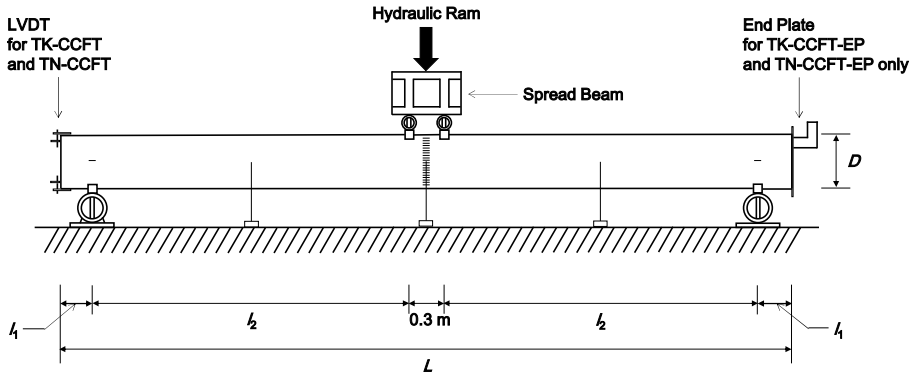

Figure 3-9 Test setup for all five specimens in this current test program

Table 3-5 Dimension of several span lengths in Figure 3-9

	Span lengths for each part		
Specimen	l_1 [mm]	l_2 [mm]	L [mm]
TK-CCFT	279.40	2768.60	6400.80
TK-CCFT-EP	76.20	2844.80	6146.80
TN-CCFT	127.00	2768.60	6096.00
TN-CCFT-EP	139.70	2844.80	6121.40

3.2 Assessment of experimental results

This section describes all the data for investigating the flexural behavior of the five specimens. Like many prior researches, the results of this current program showed the common flexural behavior features of CCFT of better moment strength and deflection compared with unfilled steel tube, upward shift of

plastic neutral axis, and concrete push-out. The end plate effect on the flexural behavior of CCFT was investigated in this section.

3.2.1 Moment-mid span deflection

Figure 3-10 shows the load history of each specimen, while **Table 3-4** shows the exact results of the maximum applied moment and deflection at mid-span. **Table 3-4** shows that in comparing the peak moments obtained for TK-CHT and TK-CCFT, a flexural capacity increase of about 36% was gained due to the concrete filling. Moreover, comparing TK-CCFT and TK-CCFT-EP, the flexural strength capacity and deflection capacity were increased slightly, so for thick CCFT beams, the end plate seems to work. However, comparing TN-CCFT and TN-CCFT-EP, the deflection capacity increased, but the flexural strength capacity decreased, so for thin CCFT beams, the end plate effect seems not to be clear.

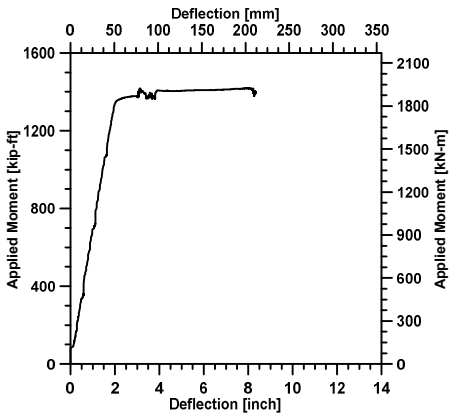

(a) TK-CHT

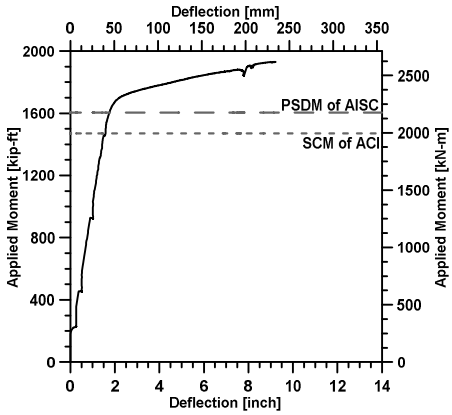

(b) TK-CCFT

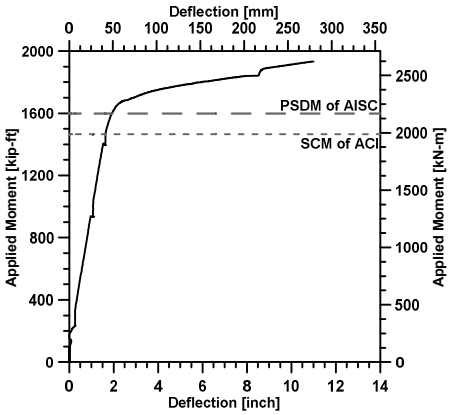

(c) TK-CCFT-EP

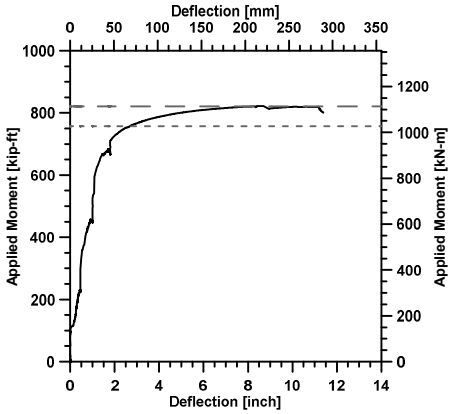

(d) TN-CCFT

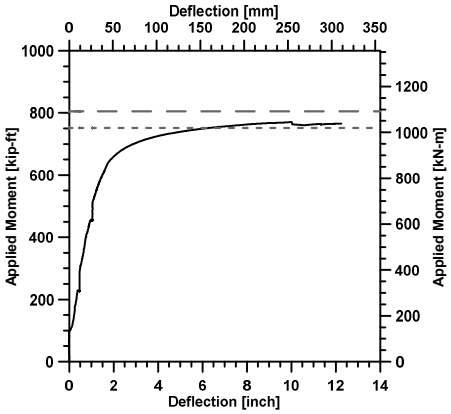

(e) TN-CCFT-EP

Figure 3-10 Applied moment vs deflection graph of each specimen

Table 3-6 Maximum applied moment and mid-span deflections

Specimen	Maximum Applied moment [kN-m]	Maximum mid-span deflection [mm]
TK-CHT	1924.19	224.79
TK-CCFT	2619.46	236.22
TK-CCFT-EP	2621.84	282.19
TN-CCFT	1115.47	291.85
TN-CCFT-EP	1045.21	352.04

For TK-CHT, the specimen was loaded four times. The first loading period was stopped because of reaching the limit on the load cell, and during the second loading period, the section became plastic at approximately 1824 kN, and loading began to plateau at 1868 kN. However, it was decided to stop this second period, and move the rollers of the spreader beam 38 mm inward to increase the applied moment. The third loading period for TK-CHT was stopped again, because complications arose with the pump, and loading decreased fairly quickly from 1868 kN to 1690 kN, after which no increase in load could be achieved. The final loading was done with safety concerns, when local outward buckling was observed near the south cradle support, as shown in **Figure 3-11**. However, no major complication arose during the last loading period, and the specimen recorded 1923.32 kN-m maximum applied moment, and 225 mm maximum deflection. At this period, the shear span was 4.4 m, with a constant moment region of 1.5 m.

Figure 3-11 Buckling near the southern loading point for TK-CHT

According to the test of TK-CHT specimen, it was decided to test all other specimens with a constant moment region of 0.3 m and with an increased shear span. The reason for this decision was to increase the available applied moment. A new spreader beam was constructed, which was shorter, measuring 0.61 m long.

For TK-CCFT, due to the high load needed from the hydraulic ram, testing of this CCFT beam was performed on two separate days. This was to let the

hydraulic ram cool, as it was unable to sustain high loads for long periods at a time. The specimen recorded a maximum moment of 2618.28 kN-m and a maximum mid-span deflection of 236 mm. During the period, steel buckling occurred at the loading points, as shown in **Figure 3-12**.

Figure 3-12 Local buckling near the loading points for TK-CCFT

Specimen TK-CCFT-EP was loaded the same as specimen TK-CCFT, and recorded a maximum moment of 2620.67 kN-m and a maximum mid-span deflection of 282 mm.

For TN-CCFT, the specimen was loaded twice but no complications arose during bending, and it was loaded smoothly. The specimen recorded a maximum moment of 1114.97 kN-m and a maximum mid-span deflection of 292 mm. However, the specimen showed outward buckling between the loading points, as shown in **Figure 3-13**.

Figure 3-13 Local buckling between the loading points for TN-CCFT

For TN-CCFT-EP, the specimen was also loaded twice, but there was no problem. The specimen recorded a maximum moment of 1044.74 kN-m and a maximum mid-span deflection of 352 mm. However, tearing occurred at a deflection of 323 mm, and outward buckling also occurred between the loading points, as shown in **Figure 3-14**.

Figure 3-14 Local buckling and tearing for TN-CCFT-EP

3.2.2 Upward shift of plastic neutral axis

Figure 3-15 shows the change of strains at each position from nineteen strain gauges. The figure shows that the plastic neutral axis (PNA) moved during the bending test. The PNA for TK-CHT was positioned at mid-depth first, and there is no shift toward the compression flange. However, the PNA for TK-CCFT was located at 10.16 mm above the mid-depth when the applied load is 20 % of the peak moment, and rose 30.48 mm upward. The PNA for TK-CCFT-EP was also at 20.32 mm above the mid-depth when the applied load is 20 % of the peak moment, and rose to 24.13 mm upward as the section became plastic. Like thick-walled CCFT specimens, the PNA for TN-CCFT was at the distance of 66.04 mm above the mid-depth at the initial stage, and rose 15.24 mm upward. The PNA for TN-CCFT-EP was at 50.8 mm above the mid depth when the applied load is 20 % of peak moment, and rose 20.32 mm upward. These movements of the PNA were seen at the moment of 90% of the peak-measured moment, and **Table 3-5** summarizes the movement of the PNA.

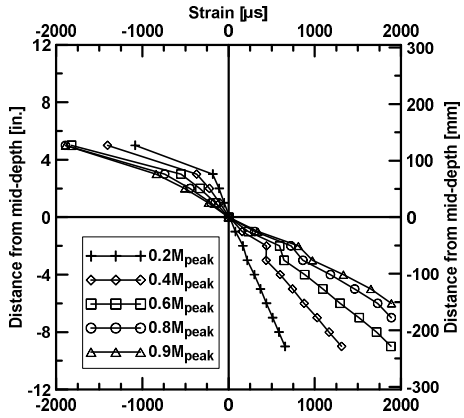

(a) TK-CHT

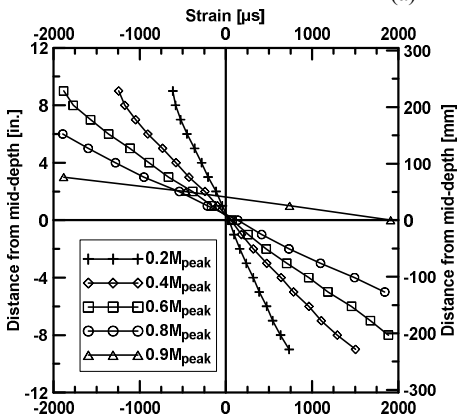

(b) TK-CCFT

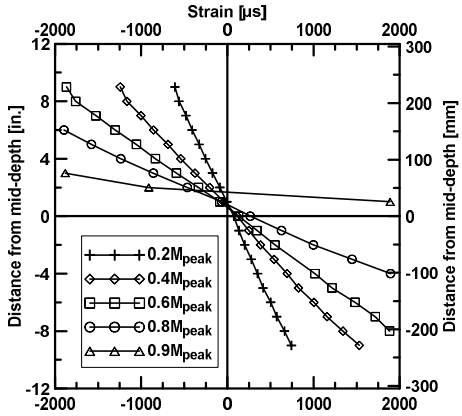

(c) TK-CCFT-EP

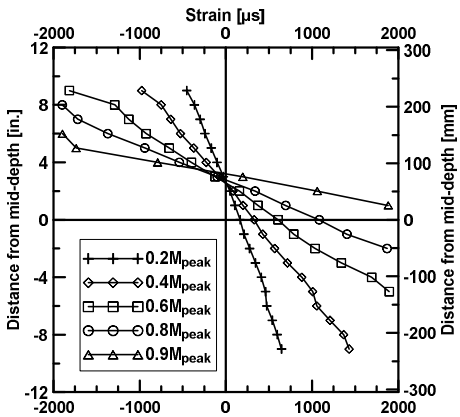

(d) TN-CCFT

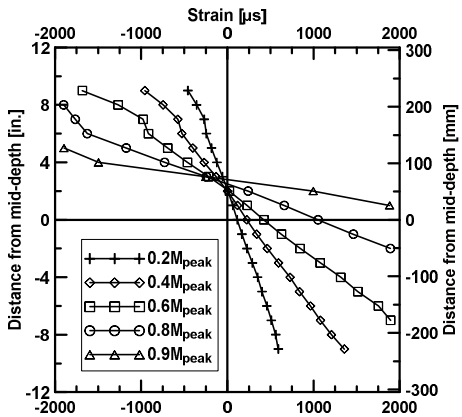

(e) TN-CCFT-EP

Figure 3-15 Neutral axis location at each load step

Table 3-7 The movement of plastic neutral axis of each specimen

Location of PNA	TK-CHT [mm]	TK-CCFT [mm]	TK-CCFT-EP [mm]	TN-CCFT [mm]	TN-CCFT-EP [mm]
20 % of M_{peak}	0	10.16	20.32	66.04	50.80
90 % of M_{peak}	0	40.64	44.45	81.28	71.12

*the distance was measured from the mid depth of circular hollow tube and circular concrete filled tubes toward the compression flange

3.2.3 Concrete push-out

Figure 3-16 shows the concrete push-out of TK-CCFT specimen. This figure shows that when the loading continued the concrete push-out increased, while relatively little concrete movement occurred along the northern end, compared to the southern end, during the whole loading periods.

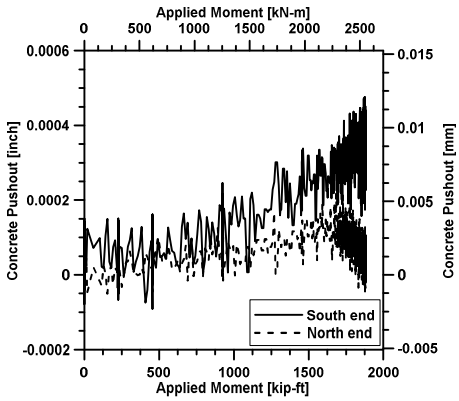

(a) 1st loading period

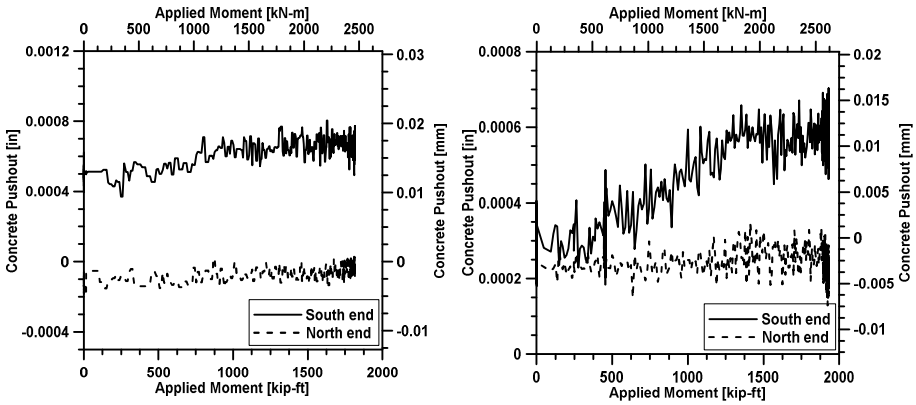

(b) 2nd loading period (c) 3rd loading period

Figure 3-16 Concrete pushout for TK-CCFT at each loading period

Figures 3-17 and **3-18** show the concrete push-out of TN-CCFT. Like TK-CCFT specimen, for TN-CCFT specimen relatively little concrete push-out occurred along the northern end, compared to the southern end. However, for TN-CCFT, almost no push-out was noticed for the northern end. Moreover, at the first loading period, concrete push-out is shown to steadily increase until 1016.82 kN-m, where an exponential-like increase is observed for the southern end. Therefore, the concrete push-out occurred more dramatically in thin-walled CCFT, than in thick-walled CCFT.

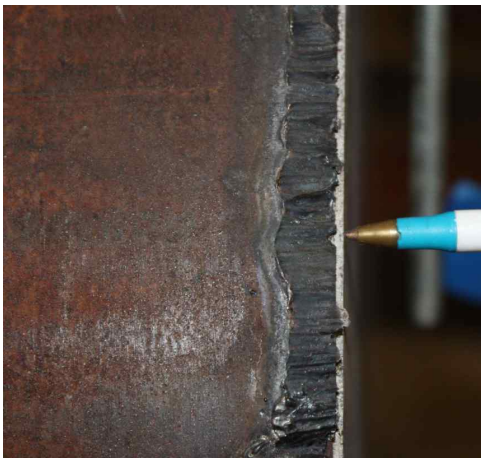

Figure 3-17 Concrete pushout for TN-CCFT

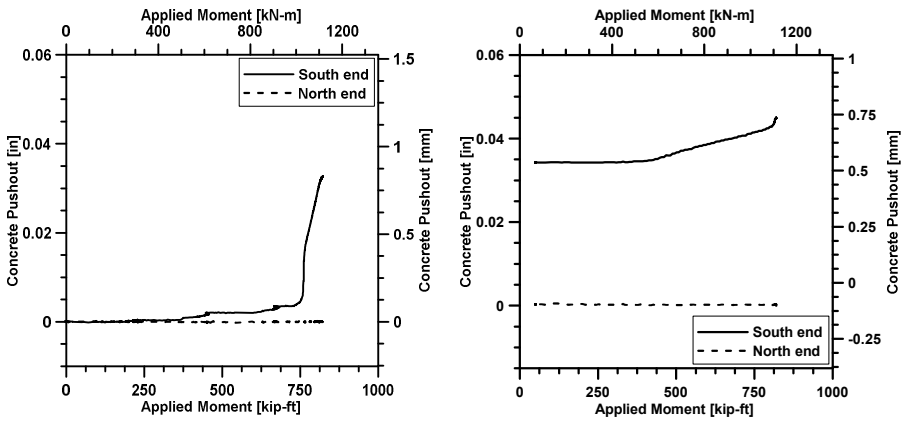

(a) 1st loading period (b) 2nd loading period

Figure 3-18 Concrete pushout for TN-CCFT at each loading period

3.2.4 End plate effect

Figure 3-19 shows the comparison of the end strains for thick-walled CCFTs and thin-walled CCFTs. The average tensile strains were calculated by averaging the strains measured at the northeast and northwest, and the southeast and southwest locations. The maximum tensile strain of 22 με was measured

for the north end of TK-CCFT, while a maximum tensile strain of 108 με was recorded for the southern end of TK-CCFT-EP. The increase in tensile strains are possibly due to the addition of forces applied at the end plates, caused by the concrete wanting to push-out.

However, no beneficial attributes were observed for the thin-walled CCFT with end plates, as a decrease in ductility was encountered, much like that for thick CFTs. When comparing the average strains at the end, no significant increase was observed for the thin-walled CCFT with end plates. The strain behavior was similar for both thin-walled CCFTs. A maximum tensile strain of 116 με was recorded in the south end of TN-CCFT, compared to a strain of 107 με for the north end of TN-CCFT-EP.

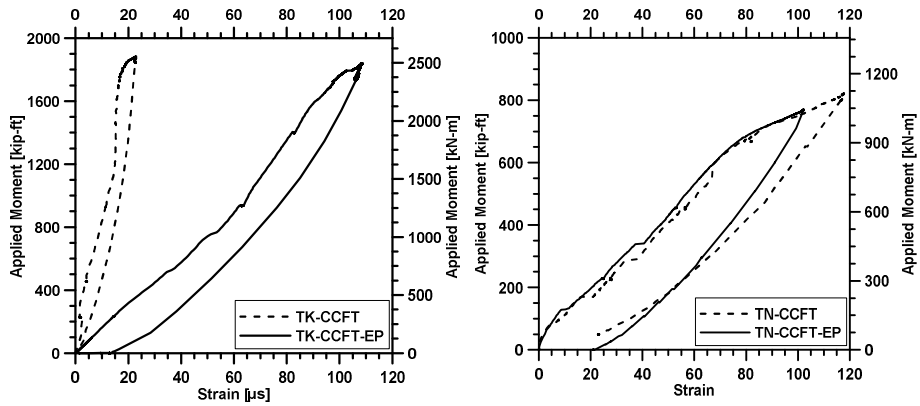

(a) For thick-walled CCFTs (b) For thin-walled CCFTs

Figure 3-19 Comparison of average tensile strains for each specimen

As a result, there is difference of strains near the reaction points by the end plate for thick-walled CCFTs, but there is no difference of strains near the reaction points by the end plate for thin-walled CCFTs. Thus, according to the thickness of steel tubes for CCFT, the end plate differently affects the flexural behavior of the CCFT. **Figure 3-19** shows two lines in each graph. The reason for this is that one line represents loading, while the other line represents unloading.

3.2.5 Stiffness

The effective stiffness of the CCFT is the significant material property for investigating the deflections, buckling, and serviceability criteria. **Figure 3-20** shows the measured moment moment-to-curvature graphs of each CCFT specimen. The slope of these graphs represents the effective stiffness of specimens, so from these data, the effective stiffness, *EI*, can be provided, as shown in **Table 3-8**.

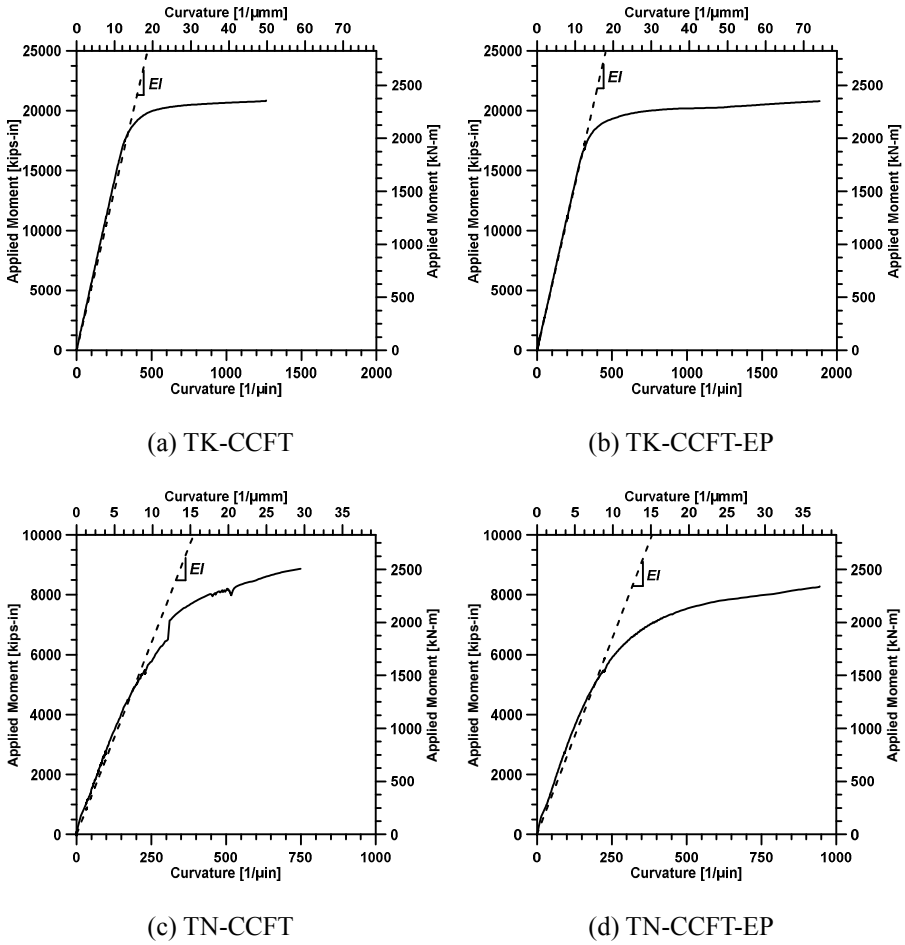

(a) TK-CCFT (b) TK-CCFT-EP

(c) TN-CCFT (d) TN-CCFT-EP

Figure 3-20 Applied moment to curvature graphs of each specimen

Table 3-8 also shows the calculated effective stiffness of CCFTs, and the

comparison with the measured effective stiffness of CCFTs. The effective stiffness of CCFTs can be calculated by several design codes, but three codes that are addressed in this study provide different equations, as follows. The first equation is from the ACI:

$$EI = \frac{\left(E_c I_g / 5\right)}{1 + \beta_{dns}} + E_s I_{sx} \quad \text{(ACI Provisions)} \tag{3-1}$$

where β_{dns} represents the ratio used to account for reduction of stiffness according to the ACI code.

The second equation is from the AISC:

$$EI = E_s I_s + C_3 E_c I_c \quad \text{(AISC Provisions)} \tag{3-2}$$

where C_3 represents the coefficient for calculation of the effective rigidity of filled composite members, which can be calculated by the following equation:

$$C_3 = 0.6 + 2\left[\frac{A_s}{A_c + A_s}\right] \leq 0.9 \tag{3-3}$$

The third equation is form the Eurocode 4:

$$EI = E_a I_a + K_e E_{cm} I_c \quad \text{(Eurocode 4 Provisions)} \tag{3-4}$$

where K_e means the correction factor to be used in the design of composite members and it is the same as in the following equation:

$$K_e = 0.6 \tag{3-5}$$

From **Eq. (3-1)** to **Eq. (3-5)**, E_a and E_s mean the Young's modulus of steel, E_c and E_{cm} mean the modulus of elasticity of concrete, I_s and I_{sx} mean the moment of inertia of structural steel tube, and I_c and I_g mean the moment of inertia of concrete. The only difference between each code relating to the effective stiffness is a constant for the concrete component. The ACI code sets the concrete constant with the least value as 0.2, the Eurocode 4 sets it as 0.6, and the AISC code sets it with the largest constant, which means more than 0.6. Therefore, as the calculated to the measured stiffness ratios show in the last columns of **Table 3-8**, ACI, AISC, and Eurocode 4 mostly overestimate the effective stiffness, but AISC code designs the least conservatively, while the ACI code designs the most conservatively among the addressed codes.

Table 3-8 Calculated and measured stiffness of each specimen

	Calculated [kN-m^2]			Measured [kN-m^2]	Calculated/Measured stiffness ratio		
Specimen	ACI	AISC	EC4		ACI	AISC	EC4
TK-CCFT	154,774	180,155	172,979	151,567	1.02	1.19	1.41
TK-CCFT-EP	153,668	178,798	171,693	156,540	0.98	1.14	1.10
TN-CCFT	79,828	105,983	102,694	73,332	1.09	1.45	1.40
TN-CCFT-EP	83,188	109,540	105,893	77,648	1.07	1.41	1.36

Figure 3-21 shows clearer that the calculated effective stiffness by each code is overestimated. Furthermore, the reason that the equations for estimating the effective stiffness are not fitted to the measured effective stiffness, indicates that there is a need to revise the equations for estimating the effective stiffness of CCFTs. As mentioned above, the reason for overestimation is from the constant for the concrete component, so it is necessary to reduce the scale of the component of the concrete effect. Therefore, this study suggests 0.12 for the constant of the concrete component to estimate the effective stiffness of the CCFT without axial loads, as shown in **Eq. (3-6)**. The 0.12 is settled by averaging the results of the current test program that is dealt with in this study.

$$EI = E_s I_s + 0.12 E_c I_c \tag{3-6}$$

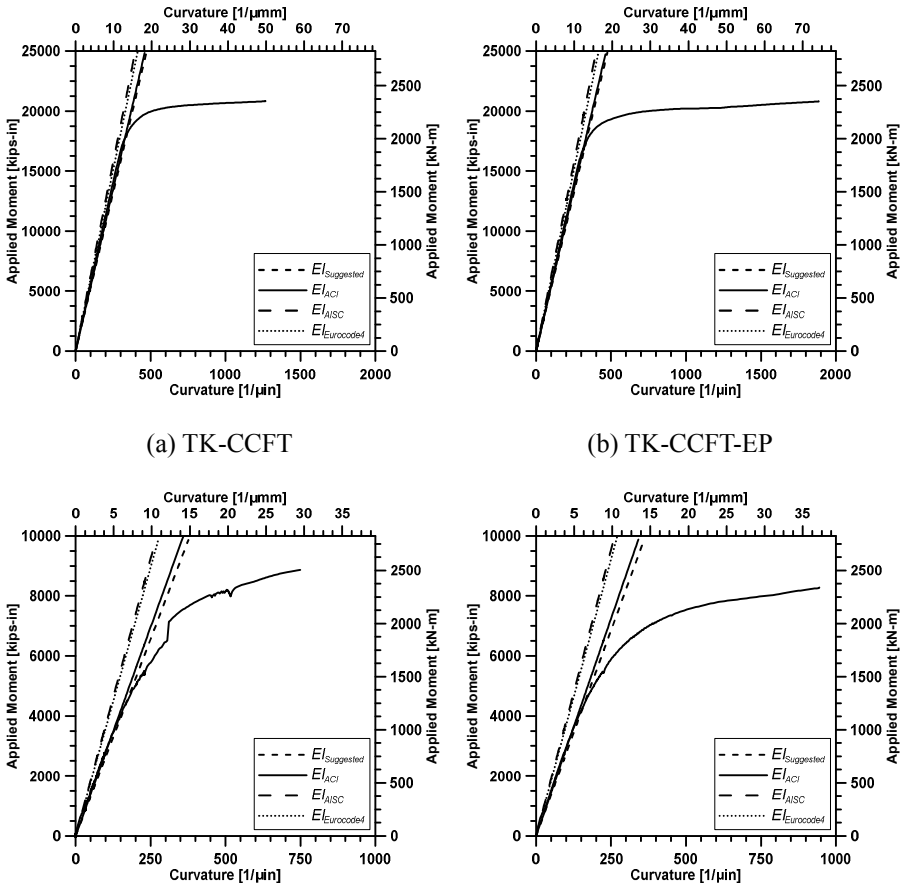

(a) TK-CCFT (b) TK-CCFT-EP

(c) TN-CCFT (d) TN-CCFT-EP

Figure 3-21 Comparison of effective stiffness according to each code

3.3 Summary

This chapter includes the assessment of the current test data and the results of the assessment. Five specimens which consist of one hollow steel tube as a

control group and four thick- and thin- walled CCFT specimens are used to understand the flexural behavior of CCFT without axial loads. Comparing to the same thickness of hollow steel tube, the CCFT specimens showed the larger flexural capacity and consistent flexural behavior such as upward shift of plastic neutral axis, concrete push-out with CCFTs which have no end plates, outward buckling near the loading points and rupture of steel in the tension zone. Furthermore, there were different characteristics between thick- and thin-walled CCFTs. For example, when the thickness was smaller, the maximum deflection prior to failure increased but the flexural capacity and the effective stiffness decreased. In addition, if the CCFTs had the end plate, the maximum deflection prior to failure increased but the effective stiffness decreased. However, the flexural capacity was not affected by the existence of end plates.

Chapter 4. Nominal Flexural Capacity of CCFT and Comparison with Test Results

This chapter focuses on the flexural capacity of CCFT. Many codes have been available to estimate the nominal flexural capacity of CCFT but the estimating methods of those codes are inconsistent. The first section is arranged to figure out the differences between them, and next section proposes and explains the newly proposed program to calculate the flexural capacity of CCFT according to each method. After that, this study also proposes the design aid graphs for estimating the flexural capacity of CCFT which are applied by the preliminary proposed program for convenience and accuracy. Next, the tests from previous published researches are shown to compare the measured and calculated flexural capacity of CCFT and the overall comparison results are presented in the end of this chapter.

4.1 Review on design codes

It is possible to design and estimate the flexural capacity of CCFT by many available codes as mentioned above. However, not only those methods have different theories and assumptions, but also those are distinct each other depending on the countries. Thus, the calculated flexural moment capacity of the CCFT beam-columns without axial force differs relying on the design methods. In this study, the limited numbers of methods such as ACI, AISC, and Eurocode 4 are dealt with because these are commonly used in the world.

First, in the United States, both ACI 318-14 and AISC-LRFD specification are used as design methods for composite members such as CCFT beam-columns which are addressed in this study. While ACI 318-14 offers simply one method

which is the strain compatibility method (SCM), AISC offers two methods which are the SCM and the plastic stress distribution method (PSDM). However, the SCM of ACI is totally same with the SCM of AISC as it is written in AISC specification which is one of two methods that AISC offers. The SCM of ACI and AISC presumes CCFT as reinforced concrete (RC) by substituting steel tube for the equal amount of reinforcement steel bars. The flexural capacity of the CFT beam-column without any axial force is calculated with the presumption of the concrete compressive strain as 0.003. In addition, the ACI method presumes that the shapes of compressive stress distribution which is related to the concrete strain distribution are various such as rectangular or trapezoidal as referred to section 22.2.2.3 of ACI 318-14. This study applies the compressive stress distribution in rectangular shape because the rectangular shape is the most commonly and reasonably used assumption. In other words, this study applies the presumption that an equivalent rectangular stress distribution is for the compressive stress of concrete and the value of it is $0.85f'_c$ as Whitney rectangular stress distribution for the ACI method. Here, f'_c means the specified concrete compressive strength. The parameter a, which means the depth of the concrete equivalent stress block, is equal to $\beta_1 c$, but the tensile stress of concrete is ignored, where β_1 is the Whitney stress block depth factor and c is the neutral axis depth from the extreme compression fiber. On the other hand, for another material, steel is assumed to have perfectly elasto-plastic stress-strain relationship and a perfect bonding between two materials, steel tube and concrete infill.

Unlike ACI, AISC proposes two methods. The PSDM which is not proposed in ACI code is a simplified version of the SCM. According to the PSDM of AISC, the strength of the section is calculated on the basis of the plastic stress distribution and the value of compressive stress of rectangular shaped concrete infill is assumed to be $0.85f'_c$, but circular shaped concrete infill is assumed to be $0.95f'_c$. The factor 0.95 in the PSDM of AISC is different from 0.85 in the SCM of ACI and AISC. The reason of this difference is that the PSDM of AISC

takes into account the confinement effect caused by the hoop stresses in circular shaped steel tubes. The length of the concrete equivalent stress block is same with the distance from the extreme compressive fiber of concrete to the neutral axis which is different from the Whitney stress block depth. Especially, only the PSDM of AISC offers the equations for calculating the flexural capacity of the CCFT, and corresponding equations are shown as follows (AISC, 2011). For a CCFT, the flexural capacity M_n (or M_B as used in AISC) is possible to compute as:

$$M_B = F_y Z_{sB} + \frac{0.95 f_c^{'} Z_{cB}}{2} \tag{4-1}$$

where F_y, Z_{sB}, f'_c, and Z_{cB} denote the yield strength of steel tube, the plastic section modulus of steel tube at point B where no axial load is applied to the CCFT as shown in **Figure 4-1-(a)**, the compressive strength of concrete, and the plastic section modulus of concrete at point B, respectively.

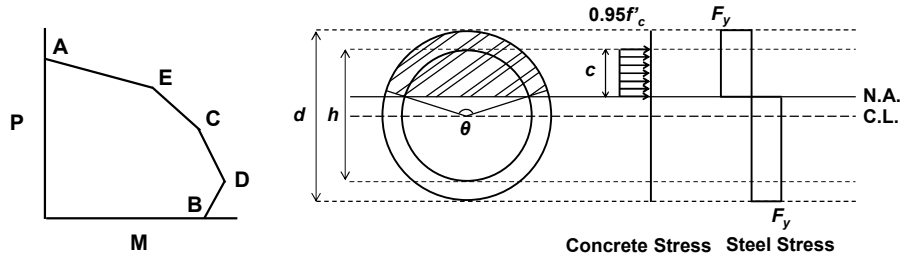

(a) P-M curve

(b) Section and stress distributions of CCFT at point B of P-M curve

Figure 4-1 Section and stress distributions of CCFT under pure bending with P-M curve

Here, Z_{sB} and Z_{cB} are also offered as follows:

$$Z_{sB} = \frac{\left(d^3 - h^3\right)}{2} \sin\left(\frac{\theta}{2}\right) \tag{4-2}$$

$$Z_{cB} = \frac{h^3 \sin^3\left(\frac{\theta}{2}\right)}{6} \tag{4-3}$$

Equations (4-2) and **(4-3)** represent that there are numerous variables: *d*, *h*, and θ. **Figure 4-1-(b)** represents these three variables, where *d* is the outer diameter of the CCFT, *h* is the diameter of the concrete component section or inner diameter of the steel tube, and θ is the angle that means the location of the plastic neutral axis at the inner face of the steel. This third variable can be computed by the subsequent equation:

$$\theta = \frac{0.0260K_c - 2K_s}{0.0848K_c} + \frac{\sqrt{\left(0.0260K_c + 2K_s\right)^2 + 0.857K_cK_S}}{0.0848K_c} \tag{4-4}$$

where

$$K_c = f_c^{'}h^2 \tag{4-5}$$

$$K_s = F_y\left(\frac{d-t}{2}\right)t \tag{4-6}$$

According to these equations, hand calculation to compute the flexural capacity of a CCFT is eventually possible but only in the PSDM of AISC. However, the remarkable thing is that the PSDM allows errors during the process of making the plastic section modulus of concrete and steel at point B, so the flexural capacity by equations in the PSDM of AISC may not be precise, but an very close value of the CCFT (Geschwindner 2010). The degree of approximation becomes greater and greater, when the CCFTs thickness is thicker and thicker.

Like AISC, Eurocode 4 also can compute the flexural capacity of the concrete

filled tube in two ways, which means the general method and the simplified method that are the strain compatibility method (SCM) and the plastic stress distribution method (PSDM), respectively. However, the SCM of Eurocode 4 differs from the SCM of AISC; and the PSDM of Eurocode 4 also differs from the PSDM of AISC.

According to Eurocode 2 Section 3.1.7, the stress-strain relations for concrete can be assumed in three different ways: parabolic, trapezoidal, or rectangular. However, this study uses the rectangular shape for concrete stress distribution duet to its most common and convenience. In the SCM of Eurocode 4, the ultimate compressive strain, uniform compressive stress, and depth of the equivalent rectangular stress distribution for concrete are various according to the compressive strength of concrete. For instance, if the concrete strength is 27 MPa, the ultimate compressive strain of concrete is 0.0035, the uniform compressive stress of concrete is f'_c, and the length of the equivalent rectangular stress distribution is $0.8c$; but if the concrete strength is 60 MPa, the ultimate compressive strain of concrete is 0.0029, the uniform compressive stress of concrete is $0.95f'_c$, and the depth of the equivalent rectangular stress distribution is $0.775c$. However, the tensile strength of concrete is ignored as any other methods, and steel is assumed to have a relationship of perfectly elasto-plastic.

The PSDM of Eurocode 4 also has some features that have similarity, and difference between the PSDM of AISC. Same as the PSDM of AISC, the PSDM of Eurocode 4 applies rigid plastic analysis, so the flexural capacity is acquired on the basis of the supposition that full interaction between the steel and concrete works. The compressive stress distribution of concrete is assumed to have an equivalent rectangular stress distribution; but the value of it is always f'_c that is difference from that for the PSDM of AISC, where its length is once again the distance from the extreme compressive fiber to the neutral axis.

4.2 Suggested program for estimating nominal flexural capacity of CCFT

Even though several methods make probable to compute the flexural capacity of CFT, it is very tough to compute the flexural capacity of CFT according to each method due to its complication and subtle differences between each method. Furthermore, it is a lot more difficult to compute that of circular sectional shaped concrete filled tube due to the shape of section. Due to this reason, there is a need to use a computer program to calculate the flexural capacity of circular concrete filled tube (CCFT) with getting exactness and ease so that a computing program is proposed in this study. The algorithm of the proposed program which is coded by MATLAB as a team effort is explained in this section.

Before starting to calculate the flexural capacity, the way of separating section should be carefully taken into account and selected for section analysis. That is because it can be a significant reason of errors by making lost or extra parts of section as in the following examples. If the sections of CCFT are cut by circular segment as shown in **Figure 4-2**, not only the extra concrete part but also the lost parts of steel are generated.

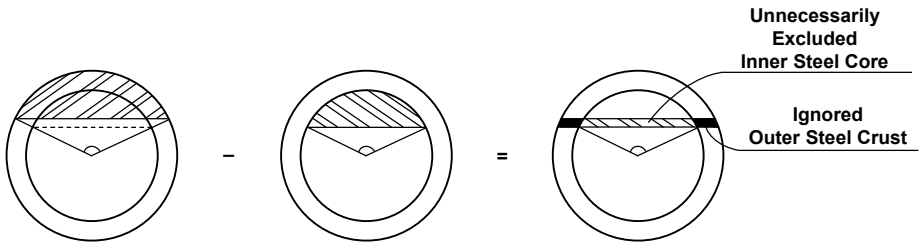

Figure 4-2 Errors caused by circular segment analysis for steel tube (modified from Geschwindner, 2010)

However, if the sections of CCFT are divided by circular sector as **Figure 4-3**, the extra concrete part is no longer generated, but both ends of steel parts are

excluded, so errors still remain.

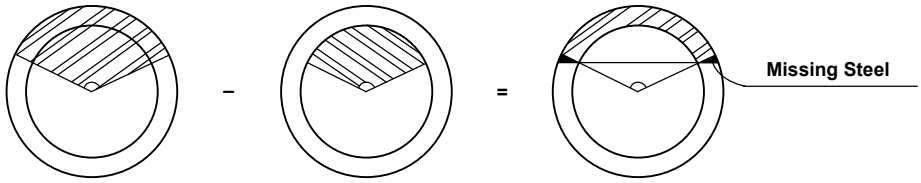

Figure 4-3 Errors caused by circular sector analysis for steel tube (modified from Geschwindner, 2010)

Thus the next approach to divide the section for sectional analysis is suggested in this study. The section is first divided by the formed materials, concrete and steel, and the steel is divided into two parts, inner steel core and total section, which is consisted of the inner steel core and outer steel crust. These three detached components of inner steel core, total section, and concrete are individually analysed, and depending on the contribution of each component, the CCFT is under the analysis as shown in **Figure 4-4**. That is the sectional analysis of the inner steel core is withdrew from that of the total section, and the sectional analysis of concrete is supplemented instead. By this means, there is no probability of getting extra or lost parts of a section, so errors can be prevented, and this is applied to make the proposed estimating program.

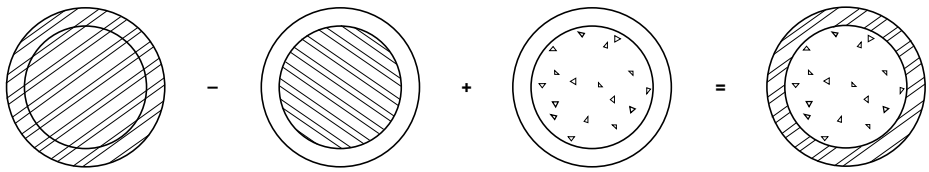

Figure 4-4 Conceptual diagram for calculating program

Figure 4-5 shows the logical flow chart estimating the flexural capacity of the CCFT that is applied to the proposed program. The starting step of the program is to enter data that are the major material properties of the CCFT by user choice. The minimum number of essential material properties to acquire the flexural

capacity is five, which are the outer steel diameter b_o, thickness of steel t, yield stress of steel F_y, Young's modulus of steel E_s, and strength of concrete f'_c. It is probable to estimate the flexural capacity of any kind of CCFT by using the proposed algorithm, because the starting step of the algorithm receives whatever material properties of CCFT a user inputs.

The subsequent step is choosing the method to evaluate the CCFT. This study deals with five methods, which are the ACI method, the SCM of AISC, the PSDM of AISC, the SCM of Eurocode 4, and the PSDM of Eurocode 4, so the proposed program is set to operate for the user to select among those five methods. After choosing the method, one is eventually ready to operate sectional analysis for calculating the flexural capacity of the CCFT.

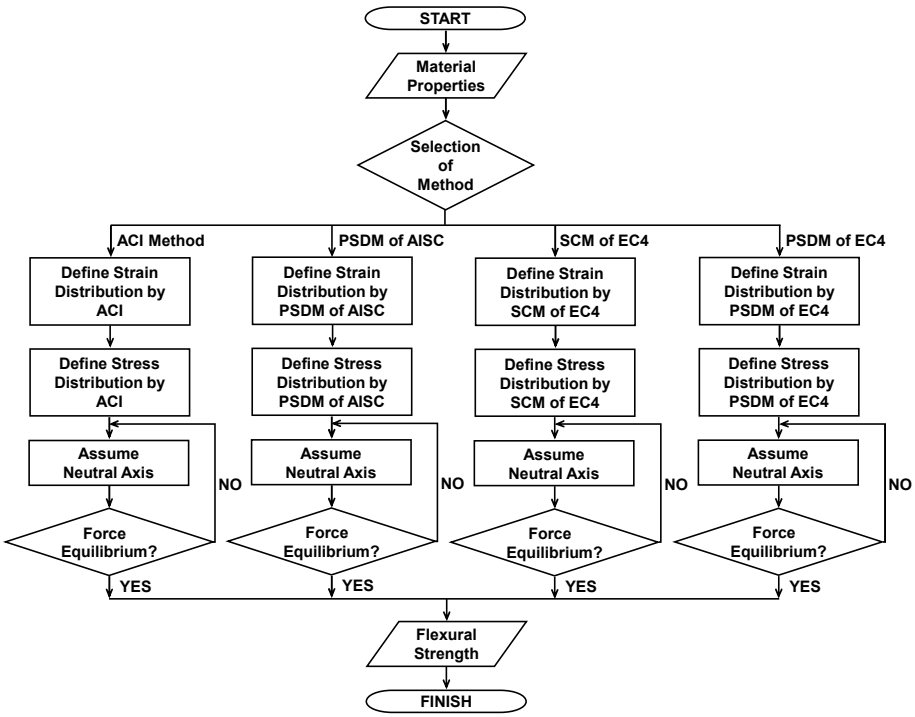

Figure 4-5 Flow chart for estimating the nominal flexural capacity of CCFT

As mentioned earlier, according to the suppositions of each method, the stress distributions of concrete and steel are various, so the proposed program is set to choose the appropriate stress distributions of concrete and steel as in **Table 4-1**. These processes that outline the strain and stress distributions are the third and fourth steps of the program, and the same processes are reran in each method according to the corresponding method.

Table 4-1 Strain and stress distributions according to each method

Method	Strain and stress distributions
ACI	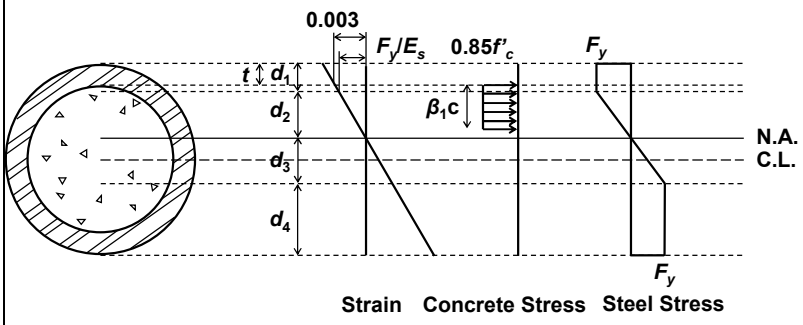
PSDM of AISC	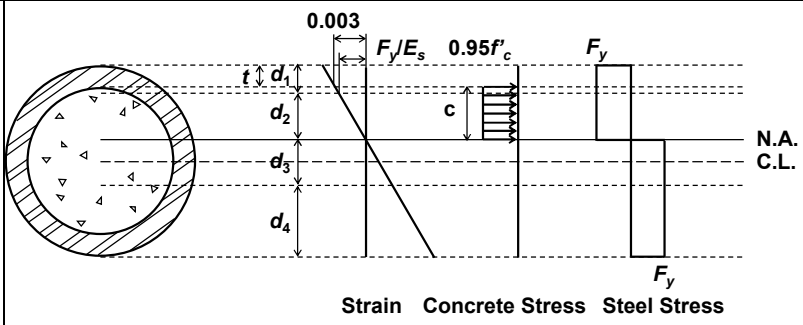
SCM of Eurocode 4	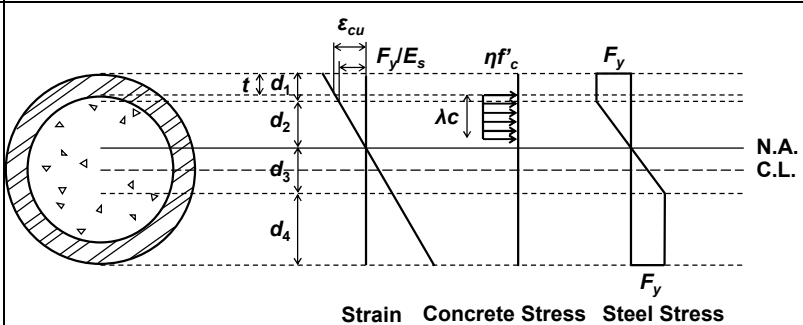

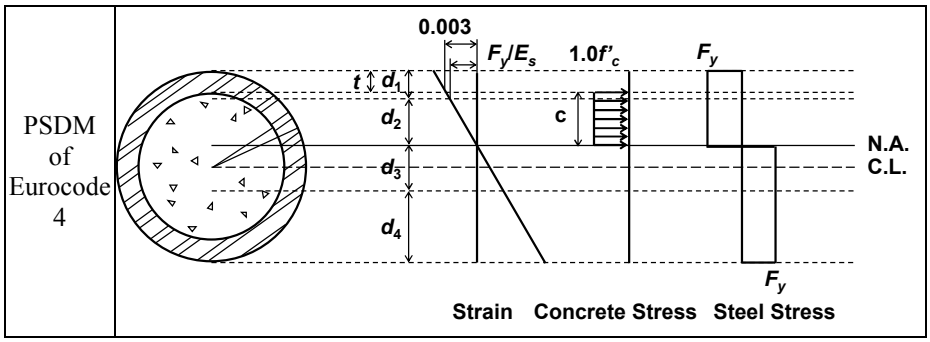

For instance, **Figure 4-6** illustrates the strain distribution and the stress distribution according to the ACI method in more detail. First of all, the steel and concrete have the same strains, and the strain distribution has linear. From this strain distribution, the stress distributions of concrete and steel can be decided. In the ACI method, while the stress distribution of concrete is assumed to be an equivalent rectangular block, the stress distribution of steel is different from that of concrete. Furthermore, the strain or stress distribution of steel can be separated out into four zones, according to the meaning of each location. The proposed program in this study utilizes these four zones in the calculating process. The first zone is from the extreme compression fiber to the point where the steel starts to yield in the compression region, and the second zone is from the end of the first zone to the neutral axis. The third zone is from the neutral axis to the point where the steel starts to yield in the tension region, and the last zone is from the end of the third zone to the extreme tension fiber. The definitions of those four zones are available not only in the ACI method, but also in any other methods.

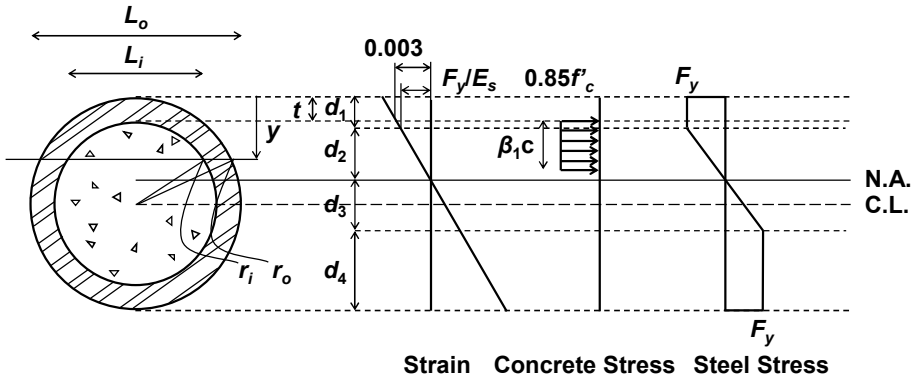

Figure 4-6 Strain and stress distributions of concrete and steel in the ACI method

Through the definitions of four zones and stress distributions corresponding to each method, the proposed program tries to calculate the neutral axis. The neutral axis is located where the sum of forces from all materials and all zones becomes zero, so the neutral axis can be mathematically found. To get all the forces from all materials and zones, the areas and stresses at the corresponding locations clearly are necessary to be determined.

Additionally, to determine the corresponding area, it is essential to know the values of variables, d_1, d_2, d_3, and d_4, which are the distances in zones 1, 2, 3, and 4, respectively. At the beginning of finding the neutral axis, d_1 is tentatively determined, and d_2 is computed by using the strain distribution. From the strain distribution, **Eq. (4-7)** below is proportionally extracted:

$$d_2 = \frac{\varepsilon_s d_1 - \varepsilon_s t}{\varepsilon_{cu} - \varepsilon_s} \tag{4-7}$$

where ε_s is the steel strain when the steel starts to yield ($\varepsilon_s = F_y/E_s$), and ε_{cu} is the ultimate compressive strain of concrete (= 0.003 in all methods, except the SCM of Eurocode 4 where ε_{cu} varies according to the compressive strength of concrete). In all methods, the value of d_3 equals that of d_2 because the

compressive and tensile behavior of steel is the same. The value of d_4 is the distance remaining after subtracting d_1, d_2, and d_3 from the total distance (the diameter of the outer steel).

The exact stresses at each location are necessary to be determined to calculate the exact forces at the locations. In the ACI method and the SCM of Eurocode 4, zones 1 and 4 are already known as they are yielded parts, so the stresses are F_y; however, the stresses in zones 2 and 3 are yet to be determined. From the stress distribution, equations for the stresses of zones 2 and 3 can be subtracted as in the following **Eq. (4-8)** and **Eq. (4-9)**. Here, a positive sign means compression and a negative sign means tension.

$$f_2(y) = F_y - \frac{y - d_1}{d_2} \times F_y \tag{4-8}$$

$$f_3(y) = -F_y + \frac{y - d_1}{d_3} \times F_y \tag{4-9}$$

For the PSDM of AISC and Eurocode 4, it is much easier to get the stress of steel than in the ACI method and the SCM of Eurocode 4. That is because steel is assumed to have a plastic stress distribution in both two methods, so only the magnitude of the yield stress of steel and the sign convention need to be taken into account.

According to the above stress and distance equations, the forces at each material and each zone can be calculated. From this procedure, the concept as in **Figure 4-4** is used to the algorithm, so the forces are computed by three imaginary components of total section, inner steel core, and inner concrete (**Table 4-2**).

Table 4-2 represents that the integral formulae with L_o and L_i, which are the chord length of the total section and that of the inner steel core as shown in **Figure 4-6**, respectively, mean the area of corresponding locations; and other

terms, such as F_y, $f_2(y)$, and $f_3(y)$ in the steel part and kf'_c in the concrete part, mean the stresses at corresponding locations.

According to the equations of **Table 4-2**, it is probable to calculate the forces from four zones of steel and concrete. As mentioned above, the program is made to individually analyse the total steel section, inner steel core, and concrete; and it then appropriately withdraws or supplements the results of sectional analysis of each material. Therefore the sum of forces is computed as in **Eq. (4-10)**, like the fundamental concept illustrated in **Figure 4-4**:

$$\begin{aligned}\sum F &= F_{outer\,steel} - F'_{inner\,steel} + F_{concrete} \\ &= \left(F_1 - F'_1\right) + \left(F_2 - F'_2\right) - \left(F_3 - F'_3\right) - \left(F_4 - F'_4\right) + F_{concrete}\end{aligned} \tag{4-10}$$

The proposed program remains iteratively operating the same procedure until the sum of the forces is zero; but after the sum of forces reaches zero, the neutral axis can be found, and the next step, which is computing the flexural capacity of CCFT without axial load case, can progress. In the same manner as computing the sum of forces, the flexural capacity of CCFT is calculated as in **Eq. (4-11)**, like the fundamental concept.

Table 4-2 Forces of steel and concrete at each zone

	SCM of ACI and Eurocode 4	PSDM of AISC and Eurocode 4
Total section (Inner steel core + Outer steel crust)	$F_1 = F_y \int_0^{d_1} L_o dy$ $F_2 = \int_{d_1}^{d_1+d_2} L_o f_2(y)\, dy$ $F_3 = \int_{d_1+d_2}^{d_1+d_2+d_3} L_o f_3(y)\, dy$ $F_4 = F_y \int_{d_1+d_2+d_3}^{2r_o} L_o dy$ where $L_o = 2\sqrt{r_o^2 - (r_o - y)^2}$	$F_1 = F_y \int_0^{d_1} L_o dy$ $F_2 = F_y \int_{d_1}^{d_1+d_2} L_o dy$ $F_3 = F_y \int_{d_1+d_2}^{d_1+d_2+d_3} L_o dy$ $F_4 = F_y \int_{d_1+d_2+d_3}^{2r_o} L_o dy$ where $L_o = 2\sqrt{r_o^2 - (r_o - y)^2}$
Inner steel core	$F'_1 = F_y \int_0^{d_1} L_i dy$ $F'_2 = \int_{d_1}^{d_1+d_2} L_i f_2(y)\, dy$ $F'_3 = \int_{d_1+d_2}^{d_1+d_2+d_3} L_i f_3(y)\, dy$	$F'_1 = F_y \int_0^{d_1} L_i dy$ $F'_2 = F_y \int_{d_1}^{d_1+d_2} L_i dy$ $F'_3 = F_y \int_{d_1+d_2}^{d_1+d_2+d_3} L_i dy$

	$F_4^{'} = F_y \int_{d_1+d_2+d_3}^{2r_o} L_i dy$ where $L_i = 2\sqrt{r_i^2 - (r_o - y)^2}$	$F_4^{'} = F_y \int_{d_1+d_2+d_3}^{2r_o} L_i dy$ where $L_o = 2\sqrt{r_i^2 - (r_o - y)^2}$
Concrete	$F_{concrete} = kf_c^{'} \int_t^{a+t} L_i dy$ where $a = \beta_1 (d_1 + d_2 - t)$ (ACI) or $\lambda (d_1 + d_2 - t)$ (SCM of EC) $k = 0.85$ (ACI) or η (SCM of EC)	$F_{concrete} = kf_c^{'} \int_t^{a+t} L_i dy$ where $a = d_1 + d_2 - t$ $k = 0.95$ (PSDM of AISC) or 1.0 (PSDM of EC)

*β_1: the factor relating to depth of equivalent rectangular compressive stress block to neutral axis depth (ACI 318-14, Section 22.2.2.4); λ: the factor defining the effective height of the compression zone (Eurocode 2 Eqs. (3.19)-(3.20)); k: the factor defining the effective magnitude of equivalent rectangular compressive stress block; and η: the factor defining the effective strength (Eurocode 2, Eqs. (3.21)-(3.22))

$$\begin{aligned} \sum M &= M_{outer\ steel} - M_{inner\ steel}^{'} + M_{concrete} \\ &= \left(M_1 - M_1^{'}\right) + \left(M_2 - M_2^{'}\right) - \left(M_3 - M_3^{'}\right) - \left(M_4 - M_4^{'}\right) + M_{concrete} \end{aligned} \tag{4-11}$$

Before estimating the flexural capacity of the CCFT, the moments of all components should be figured out, and those are shown in **Table 4-3**. Compared to the equations in **Table 4-2**, the equations in **Table 4-3** add the term ($d_1 + d_2 - y$). The new term represents the moment arm length, so the moment of each component can be induced. By using **Eq. (4-1)** and **Table 4-3**, the flexural capacity of CCFT can be estimated. The last step of the proposed program is to output this flexural capacity of the CCFT without any axial load.

Table 4-3 Moments of steel and concrete at each zone

	SCM of ACI and Eurocode 4	PSDM of AISC and Eurocode 4
Total section (Inner steel core + Outer steel crust)	$M_1 = F_y \int_0^{d_1} L_o (d_1 + d_2 - y) dy$	$M_1 = F_y \int_0^{d_1} L_o (d_1 + d_2 - y) dy$
	$M_2 = \int_{d_1}^{d_1+d_2} L_o f_2(y) (d_1 + d_2 - y) dy$	$M_2 = F_y \int_{d_1}^{d_1+d_2} L_o (d_1 + d_2 - y) dy$
	$M_3 = \int_{d_1+d_2}^{d_1+d_2+d_3} L_o f_3(y) (d_1 + d_2 - y) dy$	$M_3 = F_y \int_{d_1+d_2}^{d_1+d_2+d_3} L_o (d_1 + d_2 - y) dy$
	$M_4 = F_y \int_{d_1+d_2+d_3}^{2r_o} L_o (d_1 + d_2 - y) dy$	$M_4 = F_y \int_{d_1+d_2+d_3}^{2r_o} L_o (d_1 + d_2 - y) dy$

	where $L_o = 2\sqrt{r_o^2 - (r_o - y)^2}$	where $L_o = 2\sqrt{r_o^2 - (r_o - y)^2}$
Inner steel core	$M_1' = F_y \int_0^{d_1} L_i (d_1 + d_2 - y)\,dy$ $M_2' = \int_{d_1}^{d_1+d_2} L_i f_2(y)(d_1 + d_2 - y)\,dy$ $M_3' = \int_{d_1+d_2}^{d_1+d_2+d_3} L_i f_3(y)(d_1 + d_2 - y)\,dy$ $M_4' = F_y \int_{d_1+d_2+d_3}^{2r_o} L_i (d_1 + d_2 - y)\,dy$ where $L_i = 2\sqrt{r_i^2 - (r_o - y)^2}$	$M_1' = F_y \int_0^{d_1} L_i (d_1 + d_2 - y)\,dy$ $M_2' = F_y \int_{d_1}^{d_1+d_2} L_i (d_1 + d_2 - y)\,dy$ $M_3' = F_y \int_{d_1+d_2}^{d_1+d_2+d_3} L_i (d_1 + d_2 - y)\,dy$ $M_4' = F_y \int_{d_1+d_2+d_3}^{2r_o} L_i (d_1 + d_2 - y)\,dy$ where $L_o = 2\sqrt{r_i^2 - (r_o - y)^2}$
Concrete	$M_{concrete} = kf_c' \int_t^{a+t} L_i (d_1 + d_2 - y)\,dy$ where $a = \beta_1 (d_1 + d_2 - t)$ (ACI) or $\lambda (d_1 + d_2 - t)$ (SCM of EC) $k = 0.85$ (ACI) or η (SCM of EC)	$M_{concrete} = kf_c' \int_t^{a+t} L_i (d_1 + d_2 - y)\,dy$ where $a = d_1 + d_2 - t$ $k = 0.95$ (PSDM of AISC) or 1.0 (PSDM of EC)

*β_1: the factor relating to depth of equivalent rectangular compressive stress block to neutral axis depth (ACI 318-14, Section 22.2.2.4); λ: the factor defining the effective height of the compression zone (Eurocode 2 Section 3.1.7); k: the factor defining the effective magnitude of equivalent rectangular compressive stress block; and η: the factor defining the effective strength (Eurocode 2, Section 3.1.7)

4.3 Design aid graphs for nominal flexural capacity of CCFT

Through the proposed program with the suggested algorithm, the flexural capacity for any kind of CCFT can be estimated in any kind of methods among the five methods dealt with in this study. The following from **Figure 4-7** to **Figure 4-10** illustrates the flexural capacity of CCFTs on the bases of the ACI method (same with the SCM of AISC), the PSDM of AISC, the SCM of Eurocode 4, and the PSDM of Eurocode 4, respectively.

For each method, there are six flexural capacity versus CCFT diameter relationship graphs. Three graphs of these six graphs are divided by the concrete strength, which for one is 27 MPa, and for the other is 60 MPa. Additionally, for the same method and same concrete strength, three graphs are generated for the flexural capacities of thick-, medium-, and thin- walled CCFTs. This study

defines the thick-, medium- and thin- walled CCFTs according to their diameter to thickness ratio (D/t). The CCFTs with D/t values of 20, 35 and 50 are selected to define thick- walled, medium- walled, and thin- walled CCFTs, respectively.

Moreover, each graph has four lines, and these represent flexural strengths for the corresponding yield strengths of steel, which are 230, 250, 290, and 315 MPa according to steel grades. The range of CCFT diameters is determined on the basis of the size of steel tubes that are generally used and provided in the construction field.

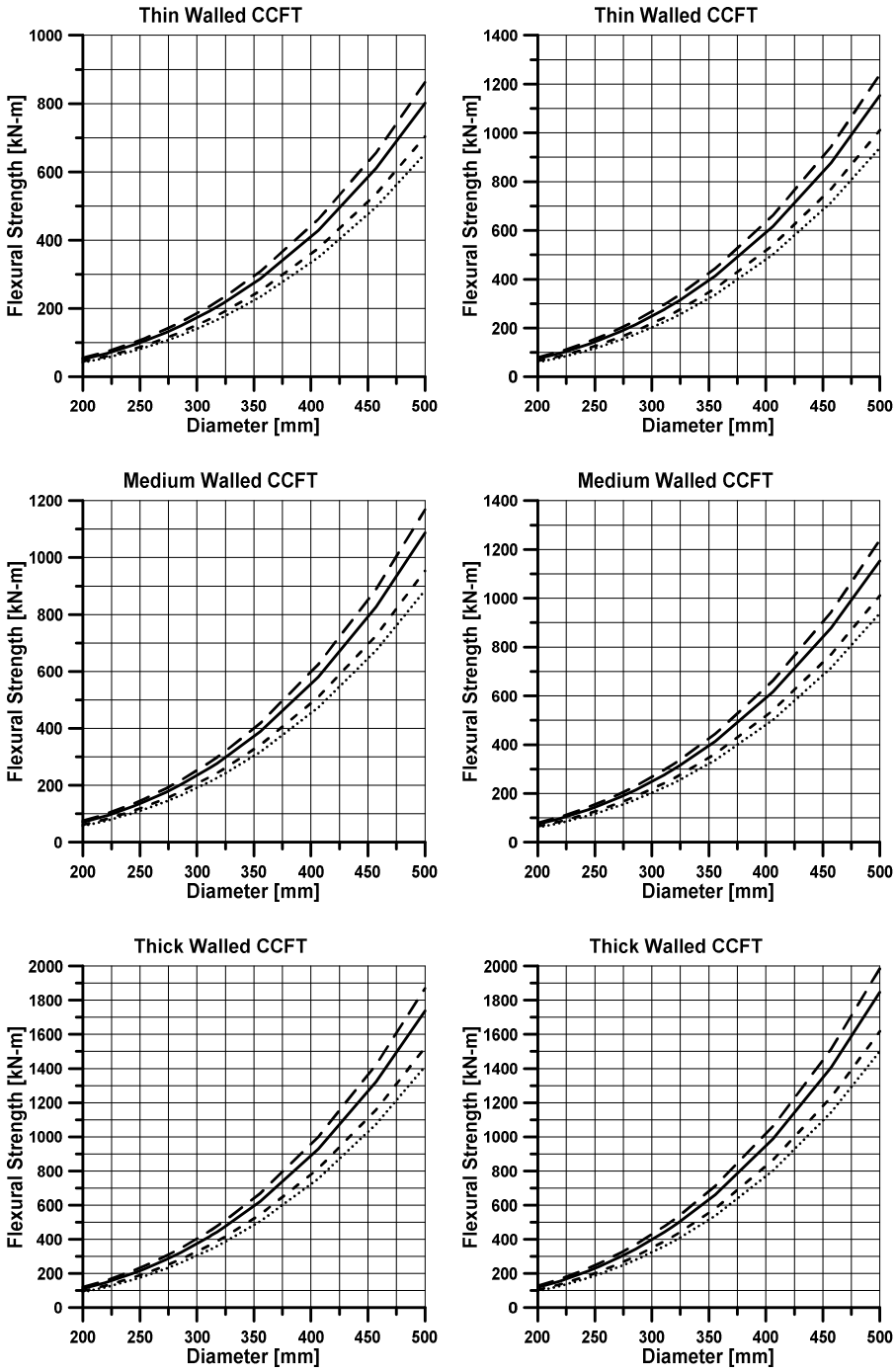

(a) f'_c = 27 MPa (b) f'_c = 60 MPa

Figure 4-7 Flexural strength-diameter graph based on the ACI method

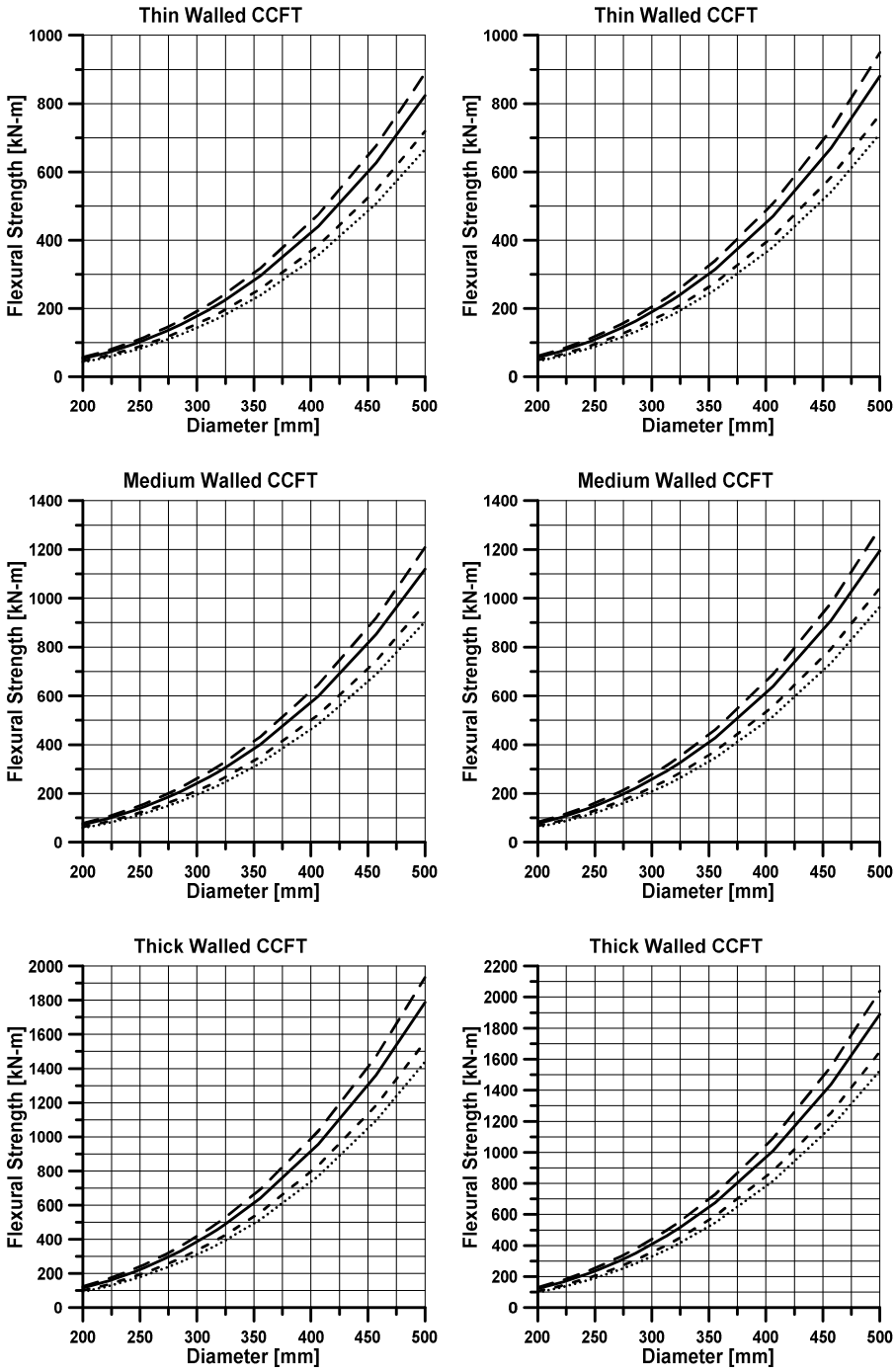

(a) f'_c = 27 MPa (b) f'_c = 60 MPa

Figure 4-8 Flexural strength-diameter graph based on the plastic stress distribution method of AISC

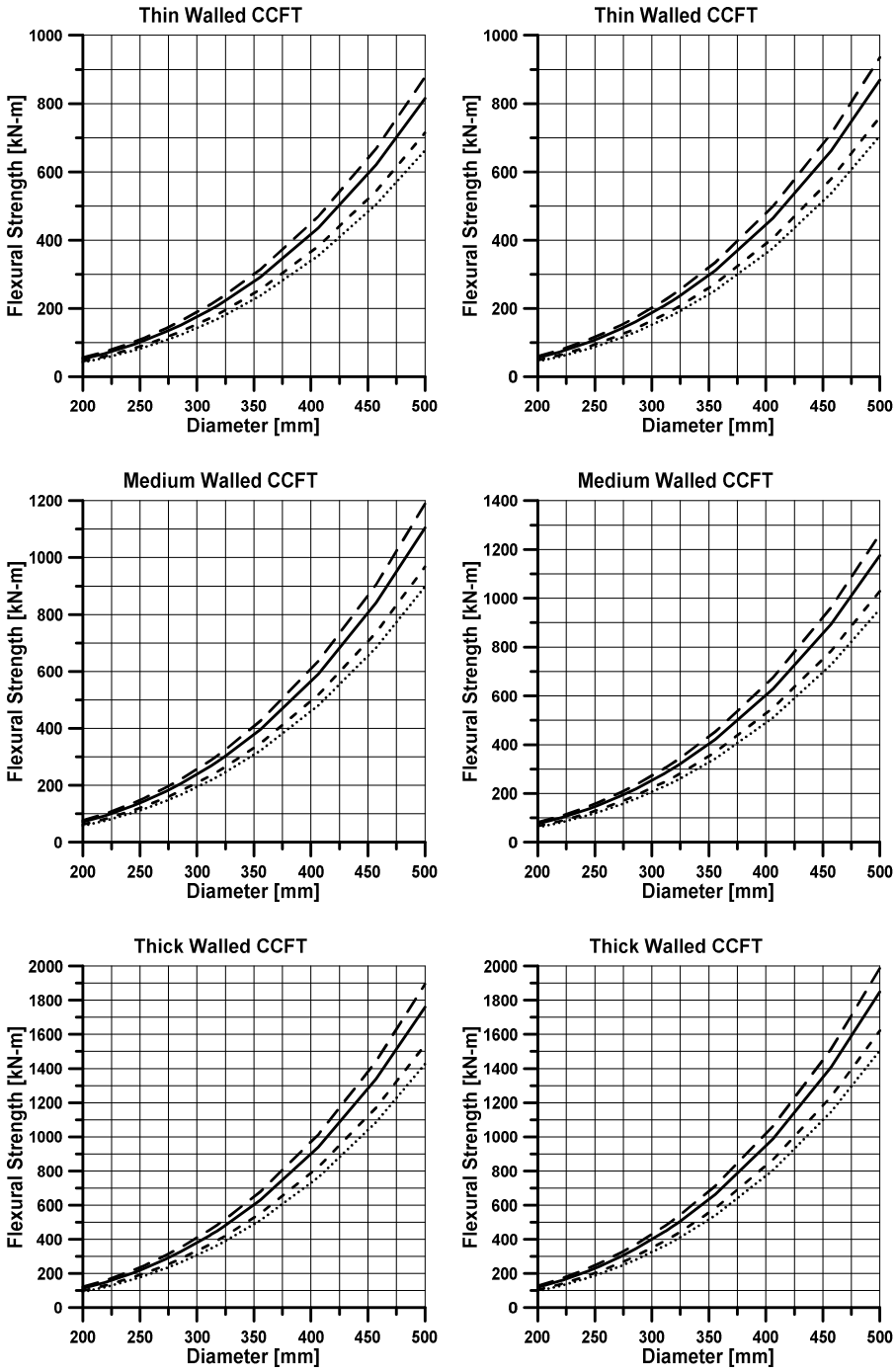

(a) f'_c = 27 MPa (b) f'_c = 60 MPa

Figure 4-9 Flexural strength-diameter graph based on the strain compatibility of Eurocode 4

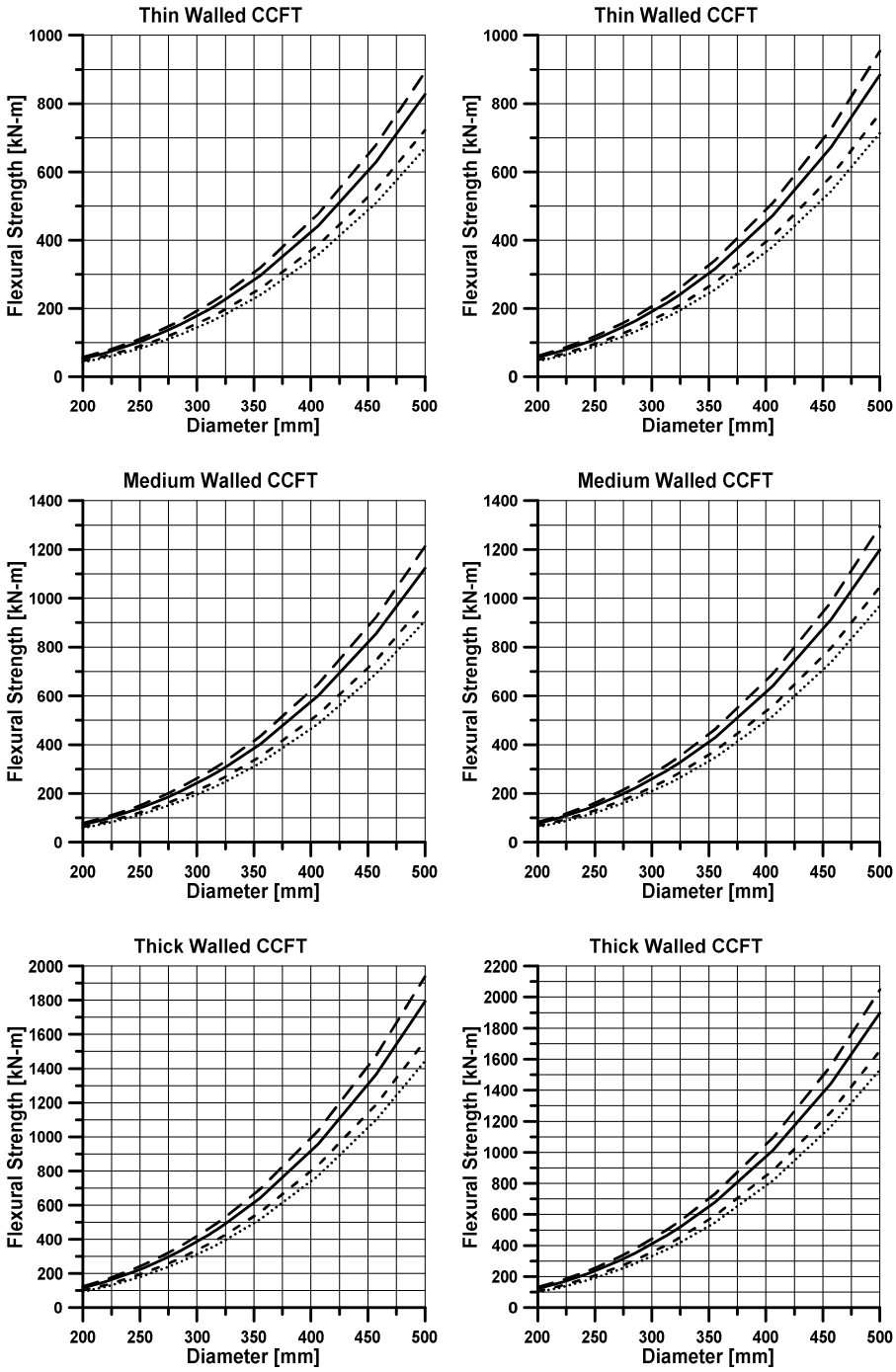

(a) f'_c = 27 MPa (b) f'_c = 60 MPa

Figure 4-10 Flexural strength-diameter graph based on the plastic stress distribution method of Eurocode 4

Figure 4-7 to **Figure 4-10** represent that if the strength of concrete is greater, the flexural capacity of the CCFT is also greater than that of the CCFT with a smaller strength of concrete. Moreover, if the thickness of steel tube is greater, the flexural capacity of CCFT is greater than that of CCFT with thinner steel tube. In other words, thick- walled CCFT has higher flexural capacity compared with medium- and thin- walled CCFT with the same other conditions. If the yield strength of the steel increases, the flexural capacity of the CCFT also increases. Similarly, if the diameter of the CCFT increases, the moment resistance value increases, but it increases almost exponentially.

When all the methods and codes are compared, the ACI strain compatibility method provides the smallest flexural capacities of CCFTs (**Figure 4-7**), while the PSDM of Eurocode 4 provides the largest values for all CCFT cases (**Figure 4-8** vs. **Figure 4-10**). Most of all, these generated twenty four design aid graphs can be used for the design of circular concrete filled tube beams at the preliminary design phase. The design aid graphs are especially useful and meaningful given that hand calculation to estimate the flexural capacity of a CCFT is very tough and even that there is no commercial software that allows such calculations.

4.4 Tests from previous experiments

To examine the proposed program and to check how different between each method, previous experiments are compiled. However, most of experiments and researches have been focused to the columns and/or beam-columns which mainly sustain the compressions and very few researches were carried out for the beams in pure flexure. This is due to the high degree of efficiencies of CFT members in resisting the compressive forces. Only a few pure bending tests have been carried out in order to investigate the strength that represents a point in the x-axis among the various combinations of axial load (P) and bending

moment (M) in P-M interaction diagram (Furlong, 1967; Tomii and Sakino, 1979; Prion and Boehme, 1994; Lu and Kennedy, 1994; Elchalakani et al., 2001; Han et al., 2006, Roeder et al., 2009; Chitawadagi and Narasimhan, 2009; Deng et al., 2010). Researches on the pure bending tests were also conducted to investigate the flexural behavior of "full scale" CFT beams under pure bending moment (Wheeler and Bridge, 2004; Probst et al., 2010).

These compiled prior experiments for analysis includes all the specimens about flexural capacity of CFT member under pure bending after the beginning research by Furlong (1967). Some previous tests are excluded if the specimens were out of the standard size or made by exceptional fabrication methods.

The specimens from Elchalakani et al. (2001) are excluded because the specimens employed about 100 mm pipes which were ultraminiature size pipes. The specimens from Han et al. (2006) and Deng et al. (2010) also are excluded. The reason of the exclusion is that the specimens from those researchers used the unusual concrete such as consolidating concrete. The test data from Roeder et al. (2009) and Chitawadagi and Narasimhan (2009) are ruled out. The cause of this exemption is that the specimens were fabricated by a spiral welding which is an exceptional fabrication method.

On the other hand, an experimental database compiled by Prion and Boehme (1994) included 26 tests but many of those tests except 2 tests are deemed excluded for inclusion because they were tests both under pure axial compression and various combinations of axial load and bending. Experimental data accumulated by Mohri et al. (2001) included 24 tests but only 6 tests are reviewed in this study because other 18 specimens had rectangular sections or had no concrete filled and inserted one or two extra steel tubes. Among Wheeler and Bridge's (2004) 6 tests, only 4 specimens become an object of attention in this study because 2 specimens were control group which were not filled with the concrete. Test data from Probst et al. (2010) are also used to compare the flexural strength of CCFT, but only one of four specimens is selected because

other 3 specimens had rectangular sections or shear connector which is not of consideration.

As a result, the database compiled for this study consists of 17 CCFT specimens including four specimens from current program and 13 specimens from 4 previous publications. The tube diameter varies between 5.98 and 18 in. (152 and 457.2 mm) with between 19.97 and 92.12 diameter to thickness ratio.

4.5 Comparison of experimental results and predictions

As shown in **Table 4-4**, the available design methods tend to estimate CCFTs' flexural strength conservatively, so generally the calculated nominal moment strengths of CCFT according to each method are greater than the measured moment strengths from accumulated experiments. By the ACI method, the design can be ended up most conservatively, while the flexural strength of CCFT is estimated less conservatively by the SCM of Eurocode 4, the PSDM of AISC and the PSDM of Eurocode 4 in the order named. However, the larger the size of CCFTs is which means the size becomes more similar to the actual size that is used in construction field, the less conservative the nominal moment strength is. These notable trends appeared to be clear in the current four specimens, results, as well as one test specimen result from Probst et al. (2010).

Table 4-4 Nominal moment strength of CCFT specimens

Authors	Dimension (diameter × thickness [mm×mm])	$M_{measured}$ [kN-m]	F_y [MPa]	f'_c [MPa]	Nominal moment strength ratio			
					ACI	PSDM of AISC	SCM of EC 4	PSDM of EC 4
Prion and Boehme (1994)	152 × 1.65	19	262	73	0.67	0.68	0.67	0.68
	152 × 1.65	21	328	92	0.77	0.79	0.77	0.79
Mohri et al. (2001)	200 × 3.20	87	400	50	0.67	0.70	0.69	0.70
	200 × 3.20	81	400	19	0.67	0.70	0.68	0.70
	200 × 4.50	121	400	50	0.65	0.68	0.67	0.68
	200 × 4.50	111	400	19	0.65	0.69	0.67	0.69
	200 × 6.00	153	400	50	0.65	0.69	0.67	0.69

	200 × 6.00	140	400	19	0.66	0.70	0.68	0.70
Wheeler and Bridge (2004)	406 × 6.40	489	350	40	0.87	0.90	0.89	0.90
	406 × 6.40	498	350	55	0.87	0.90	0.89	0.91
	456 × 6.40	630	350	48	0.88	0.90	0.90	0.91
	456 × 6.40	647	350	56	0.86	0.89	0.88	0.89
Probst et al. (2010)	457×12.00	735	407	22	1.12	1.19	1.15	1.19
Current Program	457×22.86	2620	472	30	0.76	0.83	0.79	0.83
	456×22.86	2622	472	30	0.76	0.82	0.78	0.83
	456×10.92	1115	455	30	0.93	0.99	0.96	1.00
	456×10.67	1044	455	30	0.98	1.04	1.00	1.04

*The calculated nominal moment strength is computed by the suggested computing program in this study.

In the current four specimens which are most similar to actual size beams, most methods lead to conservative. However, the PSDMs of AISC and Eurocode 4 do not allow for conservative design in some cases. The nominal moment strength ratio, that is the value of calculated flexural strength to measured flexural strength, for thin-walled CFT with end plate is 1.04 which is over 1.0. Even according to the SCM of Eurocode 4, the moment strength ratio is slightly over 1.0. Therefore, the margin of safety is very small when using the PSDMs of AISC and Eurocode 4 and the SCM of Eurocode 4. According to the ACI method, the nominal moment strengths of all four specimens are calculated to be smaller than the measured values, indicating that by the ACI method, the design can be most conservative. The KCI code which is used in Korea is similar to the ACI code, so the KCI method also leads to conservative design.

Figure 4-12 shows the flexural capacity ratio, the value of the measured to calculated flexural capacity, according to diameter, thickness and D/t ratios. As shown in **Figure 4-12-(a)**, when the diameter of CCFT increases toward the actual size, the flexural capacity ratio goes over 1.0. It means that the design would tend to be more unconservative when the diameter increases. Furthermore, as implied in **Figure 4-12-(b)** and **Figure 4-12-(c)**, the flexural strength of thinner walled CCFTs may be estimated more unconservatively than that of thicker walled CCFTs. This aspect probably is because for thin walled

CCFT, the confinement effect of steel is less effective than what is expected by the PSDM of AISC and Eurocode 4. These results signal that the bond stress between concrete and steel tube is not enough so the composite action was not effective.

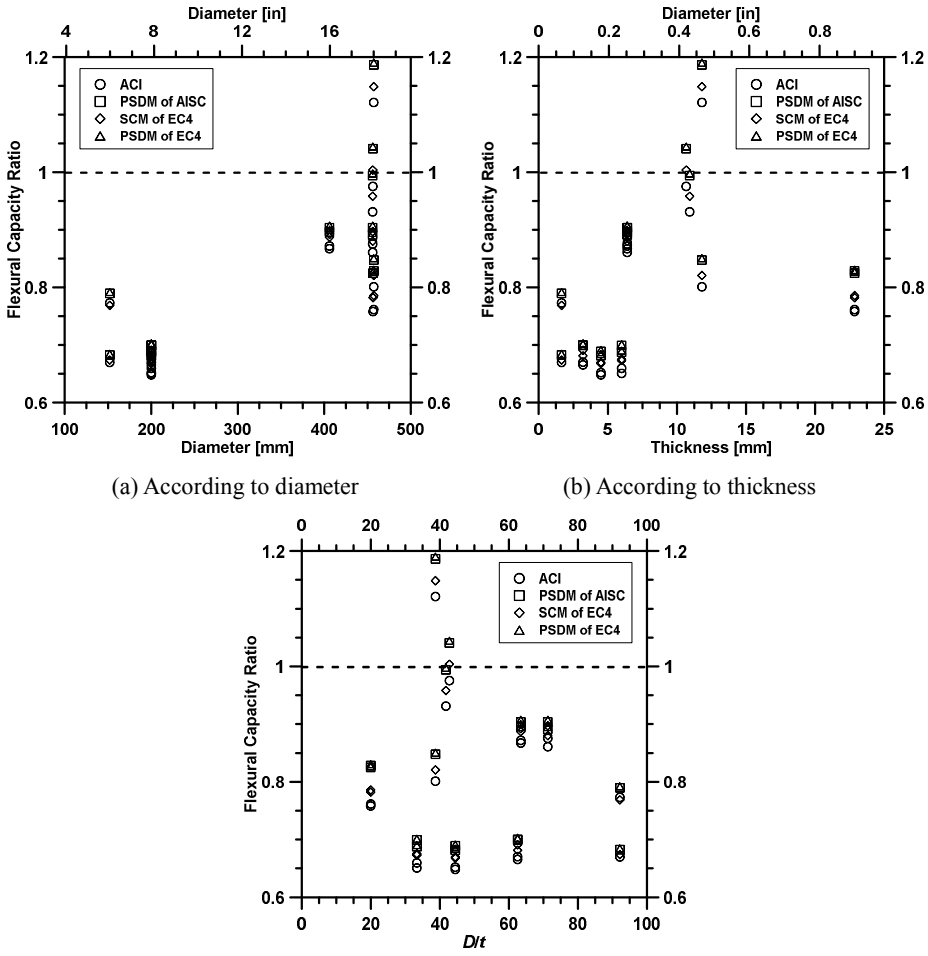

(a) According to diameter

(b) According to thickness

(c) According to *D*/*t* ratio

Figure 4-11 Flexural strength ratio according to diameter, thickness and *D*/*t* ratio

Furthermore, as shown in **Table 4-4** and **Figure 4-11**, like thin walled CCFTs of this research project, the CCFT specimen constructed by Probst et al. (2010) drew the same result that the calculated flexural strength according to each method was greater than the measured flexural strength. The specimens had

very similar diameter, thickness, and length. However, the flexural strength ratio for CCFT tested by Probst et al. (2010) was over 1.0 with larger percentage. The cause of this aspect may be the different shear span as shown in **Figure 4-12**. While the beam of Probst et al. (2010) was tested with a shear span of 2,591 mm and a pure moment region of 2,896 mm, a shear span of 5,537 mm and a pure moment region of 305 mm were used for this project. The differences in capacity are likely due to the increased frictional resistance as shown in **Table 4-5** along the shear span. Frictional resistance along the steel and concrete interface can be seen as a function of the interior surface area. As the concrete is being forced out, the significant increase in the shear span should contribute to the friction, nearly double the interior surface area for this project compared to that by Probst et al (2010). Therefore, the frictional resistance seems to be increased providing great micro-locking bond characteristics; thus, further studies with the frictional resistance would definitely be needed.

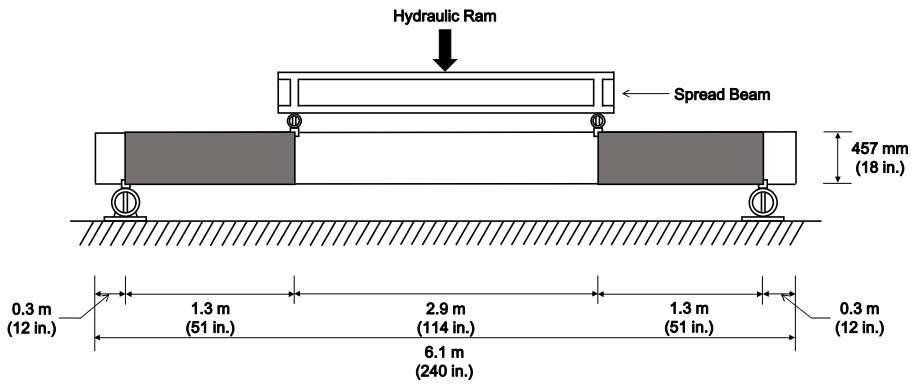

(a) Specimen C-NS from Probst et al. (2010)

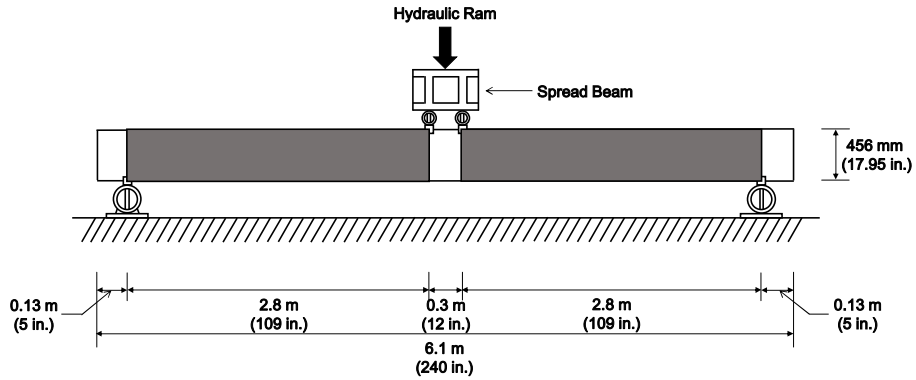

(b) Specimen TN-CCFT from the current test program

Figure 4-12 Difference specimens C-NS and TN-CCFT in terms of frictional resistance area

Table 4-5 Frictional surface area between specimens C-NS and TN-CCFT

Specimen	Frictional surface area (A) [m^2]
C-NS from Probst et al. (2010)	3.53
TN-CCFT from the current program	7.55

4.6 Summary

This chapter attempts to examine the differences of design codes concerning on the flexural capacity of CCFTs and provides the design aid program and graphs for calculating the flexural capacity of CCFTs by reflecting all differences for convenience. Additionally, it compares the flexural capacity of the experimental results and the prediction from the design aid program and graphs. For comparison, this study compiled most of previous studies regarding the flexural behavior of CCFTs including the current test program. The comparison concludes that there is a possibility to predict the flexural capacity of CCFTs unconservatively by the current design codes especially for full-scaled CCFTs. Specimen TN-CCFT-EP from the current test program which was thin-walled CCFT with end plate and Specimen C-NS of Probst et al. (2010) provide the smaller measured flexural capacity than that of prediction. From the results, not

only it is found that the full scaled CCFT may not provide the full composite plastic flexural capacity unlike the prediction, but also that the shear span is another significant variable which affects the flexural behavior. That is because those two specimens had very similar dimension such as diameter, thickness, and span length but the shear span length was the only difference between them.

Chapter 5. Conclusion

In this study, the flexural behavior of CCFT beam-columns was investigated. Five new full scaled CCFT beam specimens tested without axial loads were used to investigate and supplement or oppose previous researches which had been done with small sized CCFT specimens. Moreover, a computing program is applied to accurately calculate the flexural capacity of CCFT beams, with its new algorithm that reflects all the differences between the addressed methods. In addition, all CCFT specimens from prior researches are revisited to examine the flexural behavior of various sizes of CCFT and to compare with the currently measured flexural capacity, as well as with the calculated flexural capacity according to each method. Based on the current test results and the comparison results, the following conclusions were made.

1) As many test results from a large majority of past researches, forced outward buckling near the loading points, extrusion or push-out of the concrete at the tube ends and upward shifting of the plastic neutral axis (PNA) during tensile cracking of the concrete were exhibited in the full scaled CCFT specimens in this study.

2) From the current test results, it was possible to compare the thick-walled CCFTs and thin-walled CCFTs. As a result, thick-walled CCFTs produced the better flexural behavior than the thin-walled CCFTs. Even though thick-walled CCFTs had less maximum deflection at mid-span, the greater flexural capacity and stiffness were resulted in compared to the thin-walled CCFTs.

3) This study was also planned to examine the end plate effect on the flexural behavior. This study concluded that there was inconsistent

effects on the flexural behavior by the use of end plate. For example, the flexural capacity of thick-walled CCFT increased with end plate but the flexural capacity of thin-walled CCFT decreased. However, those variations were modest so it can be ignored. It can be concluded that the use of end plate does not affect the capacity of CCFTs much, but it has some effects on the ductility. According to the data of strains near the supports, the end plate used for thick walled CCFTs induced the larger ductility than thin walled CCFTs.

4) Based on the database of collected CCFT specimens, for the small sized CCFTs, the measured flexural strength is always much greater than the calculated flexural strength. However, for the full sized CCFT, the measured flexural strength is very similar or in some case less than the calculated flexural strength. There is some possibility that the bond stress between concrete and steel is less when the size of specimen increases, so the composite action does not fully occur. Further studies with diverse sizes of full scaled CCFTs are needed.

5) For full scaled CCFTs, the measured flexural strengths of the thin walled CCFT with end plate in the current test program and the CCFT specimen of Probst et al. (2010) are greater than the calculated flexural strength in the PSDM of AISC and Eurocode 4. However, it appears that the end plate makes the larger ductility of thick-walled CCFT. Furthermore, even though the size of the specimen of Probst et al. (2010) is very similar to the current thin walled CCFT specimen without end plate, the measured flexural strengths are fairly different. The certain difference between these two specimens is possibly due to the different shear span. The shear span for the specimen of Probst et al. (2010) is almost twice the value of thin walled CCFT without end plate from this study. Therefore, this study concludes that the frictional resistance along the shear span seems to be another significant variable to affect the flexural strength. However, there is a need to do further studies to

make sure such an effect.

References

1. ACI Committee 318 (2014), "Building Code Requirements for Structural Concrete and Commentary," American Concrete Institute, Farmington Hills, MI, USA.

2. AIJ (2001), "Standards for Structural Calculationof Steel Reinforced Concrete Structures," Architectural Institute of Japan, Japan.

3. AISC (2011), "Steel Construction Manual," American Institute of Steel Construction; Chicago, IL, USA.

4. Chitawadagi, M. V., and Narasimham, M. C. (2009), "Strength Deformation Behaviour of Circular Concrete Filled Steel Tubes Subjected to Pure Bending," *Journal of Constructional Steel Research,* 65(8-9), 1836-1845.

5. Deng, Y., Tuan, C., Zhou, Q., and Xiao, Y. (2011), "Flexural Strength Analysis of Non-Post-Tensioned and Post-Tensioned Concrete-Filled Circular Steel Tubes," *Journal of Constructional Steel Research*, 67(2), 192-202.

6. Elchalakani, M., Zhao, X. L., and Grzebieta, R. E. (2001), "Concrete-Filled Circular Steel Tubes Subjected to Pure Bending," *Journal of Constructional Steel Research*, 57 (11), 1141-1168.

7. Eurocode 2 (2004), "Design of concrete structures. Part 1.1: General rules and rules for building," European Committee for Standardization, Brussels, Belgium.

8. Eurocode 4 (2004), "Design of composite steel and concrete structures. Part 1.1: General rules and rules for building," European Committee for Standardization, Brussels, Belgium.

9. Furlong, R. W. (1967), "Strength of Steel-Encased Concrete Beam Columns," *Journal of the Structural Division*, ASCE, 93(ST5), 113-124.

10. Geschwindner, L. F. (2010), "Discussion of Reinforced Concrete Members under Flexure and Combined Flexure and Direct Compression," *Engineering Journal*, 47(2), 483-498.

11. Gho, W. M., and Liu, D. (2004), "Flexural Behaviour of High-strength Rectangular Concrete-Filled Steel Hollow Sections," *Journal of Constructional Steel Research*, 61(11), 1681-1696.

12. Guo, W. M., Zhang, S., Kim W. J., and Ranzi, R. (2007), "Behavior of Square Hollow Steel tubes and Steel Tubes Filled with Concrete," *Thin-Walled Structures*, 45(12), 961-973.

13. Han, L. (2004), "Flexural Behaviour of Concrete-Filled Steel Tubes," *Journal of Constructional Steel Research*, 60(2), 313-337.

14. Han, L., Hu, L., Yao, G., and Liao, F. (2006), "Further Study on the Flexural Behaviour of Concrete-Filled Steel Tubes," *Journal of Constructional Steel Research,* 62(6), 554-565.

15. Lee, C.-H., Kang, T. H.-K., Kim, S.-Y., and Kang, K. (2016), "Strain Compatibility Method for the Design of Short Rectangular Concrete-Filled Tube Columns under Eccentric Axial Loads," *Construction and Building Materials*, 121, 143-153.

16. Lu, Y., and Kennedy, D. (1994), "The Flexural Behaviour of Concrete-Filled Hollow Structural Sections," *Canadian Journal of Civil Engineering*, 21(1), 111-130.

17. Matsui, C., and Tsuda, K. (1987), "Strength and Behavior of Concrete-Filled Steel Square Tubular Columns with Large Width-Thickness Ratio," *Proceedings of Pacific Conference on Earthquake Engineering*, Auckland, New Zeland, 2, 1-9.

18. Mohri, E., Shioi, Y., and Hasegawa, A. (2003), "Performance of Reinforced Concrete Filled Tube for Shear Force and Bending moment," *Hachinohe Institute of Technology*, 9, 13-28.

19. Morino, S. and Tsuda, K. (2003), "Design and Construction of Concrete-Filled Steel Tube Column System in Japan," *Earthquake Engineering and Engineering Seismology*, 4, 51-73.

20. Nakamura, S., Tanaka, H. and Kato, K. (2009), "Static Analysis of Cabled-Stayed Bridge with CFT Arch Ribs", Journal of Constructional Steel Research, 65, 776-783.

21. Nghiem, A. (2011), "Flexural Behavior of Circular Concrete Filled Steel Tubes," Master's thesis, Department of Civil Engineering, University of Oklahoma, Norman, OK, USA.

22. Prion, H. G. L., and Boehme, J. (1994), "Beam-Column Behaviour of Steel Tubes Filled with High Strength Concrete," *Canadian Journal of Civil Engineering*, 21(2), 207-218.

23. Probst, A., Kang, T. H.-K., Ramseyer, C., and Kim, U. (2010), "Composite Flexural Behavior of Full-Scale Concrete Filled Tubes without Axial Loads," *Journal of Structural of Structural Engineering*, 136(11), 1401-1412.

24. Roeder, C. W., Cameron, B., and Brown, C. W. (1999), "Composite Action in Concrete Filled Tubes," *Journal of Structural Engineering*, ASCE, 125, 477-494.

25. Roeder, C. W., and Lehman D. E. (2007), "Composite Action in Concrete

Filled Steel Tubes," *Proceedings of the Pacifica Structural Steel Conference, Steel Structures in Natural Hazards,* Wairakei, New Zealand, 1, 17-29.

26. Roeder, C. W., Lehman D. E., and Thody, R. (2009), "Composite Action in CFT Components and Connections," *Engineering Journal*, Fourth Quarter, 46(4), 229-242.

27. Schneider, S. P. (1998), "Axially Loaded Concrete-Filled Steel Tubes," *Journal of Structural Engineering*, 124(10), 1125-1138.

28. Tomii, M. and Sakino, K. (1979), "Experimental Studies on the Ultimate Moment of Concrete Filled Square Steel Tubular Beam-Columns," *Transactions of the Architectural Institute of Japan*, 275, 55-63.

29. Thody, R. (2006), "Experimental Investigation of the Flexural Properties of High-Strength Concrete Filled Steel Tubes," Master's thesis, Department of Civil Engineering, University of Washington, Seattle, WA, USA.

30. Varma, A. H., Ricles, J. M., Sause, R., and Lu, L. (2002), "Seismic Behavior and Modeling of High-Strength Concrete-Filled Steel Tube Beam-Columns," *Journal of Constructional Steel Research*, 22(58), 725-758.

31. Webb, J. (1993), "High-Strength Concrete: Economics, Design, and Ductility," *Concrete International*, 15(1), 27-32.

32. Wheeler, A. and Bridge, R. (2004), "The Behaviour of Circular Concrete-Filled Thin-Walled Steel Tubes in Flexure," *Composite Construction in Steel and concrete V*, Proceeding of 5th International Conference, ASCE, Mpumalanga, South Africa, 412-423.

33. Ying, W. (2006), "Development of New CFT Column-CFT Beam Frame Structure using Self-Compacting Concrete," Ph Dissertation, Department of Enginnering, Kochi University of Technology, Kochi, Japan.

국 문 초 록

원형 콘크리트충전강관 부재의 휨강도 및 거동

합성구조는 기존의 철근콘크리트구조나 강구조와 비교하여 강도와 강성 측면에서 보다 유리하다. 이러한 구조적 장점 때문에 초고층 건물과 장경간 구조물의 수요가 늘어나는 현대에 이르러 합성구조가 널리 사용되고 있다. 합성구조의 종류는 그 형식에 따라 충전형(CFT; Concrete Filled Tube)과 매입형(SRC; Steel Reinforced Concrete)으로 크게 나뉘는데, 본 연구에서는 충전형(CFT) 구조를 다룬다. 특히 충전형 CFT 는 압축을 지배적으로 받는 기둥 부재로 주로 사용되어 왔으며, 따라서 편심의 유무에 따른 압축을 받을 때 CFT 기둥 부재의 거동에 관한 연구가 다수 수행되었다. 그러나 국내외적으로 CFT 구조가 기둥 뿐만 아니라 보로서 장경간을 요하는 건축물과 교량 등에 활용됨에도 불구하고, 이에 대한 연구는 부족한 실정이다.

지난 연구 결과, CFT 보의 거동이 속이 빈 강관의 거동과 매우 유사하다고 보고되었던 초기의 연구와는 달리(Furlong, 1967), 충전된 콘크리트가 압축 저항을 하며 중립축을 압축측으로 이동시킴으로써 거동에 영향을 미치며, 압축을 받는 강관의 국부좌굴을 방지한다는 것 등 보다 정확한 CFT 보의 휨거동에 대한

연구가 최근까지 보고되고 있다. 그러나 이들 연구의 대부분은 축소 모형으로 제작된 CFT 로 분석되었으며 실물대 크기의 실제 CFT 보의 거동에 대한 연구는 극히 부족한 상태이다. 또한, 원형 CFT(CCFT)의 경우 그 단면 형태의 특성상 세밀한 연구가 진행되어야 함에도 불구하고 이에 대한 연구는 더욱 부족한 실정이다.

따라서 본 연구에서는 실물크기 CCFT 실험 데이터를 분석하여 축력을 받지 않는 상태에서의 CCFT 의 휨거동을 연구하였다. 특히 CCFT 의 휨강도에 있어서 여러 코드별로 산정식이 존재하지만 그 방식이 동일하지 않을 뿐만 아니라, 최근 보고된 실물 크기 실험값과 비교하여 볼 때도 보수적이지 못한 설계로 이어지는 것으로 나타났다. 또한, 추가적으로 실제 측정된 CCFT 부재의 휨강도값과 코드에 따라 계산된 값을 비교 분석하였을 때 강관의 두께가 감소할 때, 즉 박판일 때 안전율이 감소하는 것으로 나타났다.

단면이 원형인 특성상 CCFT 의 휨강도를 손쉽게 계산할 수 없기 때문에, 본 연구에서는 설계자가 CCFT 부재의 물성치를 입력하여 CCFT 의 휨강도를 산정할 수 있는 프로그램을 개발하였다. 이에 더하여, 정밀한 계산과정 없이도 CCFT 부재의 휨강도를 산정할 수 있는 설계 그래프를 제시하여 보다 정확하고 편리한 설계가 가능하도록 유도하였다.

핵심용어: 원형 콘크리트충전강관, 휨거동, 휨강도
학번: 2015-21113